nature COMMUNICATIONS

OPEN

ARTICLE

Received 21 Dec 2010 | Accepted 18 Apr 2011 | Published 24 May 2011

DOI: 10.1038/ncomms1316

Circadian regulation of intracellular G-protein signalling mediates intercellular synchrony and rhythmicity in the suprachiasmatic nucleus

Masao Doi[1,*], Atsushi Ishida[2,*], Akiko Miyake[2], Miho Sato[1], Rie Komatsu[1], Fumiyoshi Yamazaki[1], Ikuo Kimura[3], Soken Tsuchiya[3], Hiroshi Kori[4,5], Kazuyuki Seo[1], Yoshiaki Yamaguchi[1], Masahiro Matsuo[1], Jean-Michel Fustin[1], Rina Tanaka[1], Yasuko Santo[1], Hiroyuki Yamada[1], Yukari Takahashi[1], Michihiro Araki[6], Kazuki Nakao[7], Shinichi Aizawa[7], Masaki Kobayashi[8], Karl Obrietan[9], Gozoh Tsujimoto[3] & Hitoshi Okamura[1,2]

Synchronous oscillations of thousands of cellular clocks in the suprachiasmatic nucleus (SCN), the circadian centre, are coordinated by precisely timed cell–cell communication, the principle of which is largely unknown. Here we show that the amount of RGS16 (regulator of G protein signalling 16), a protein known to inactivate Gαi, increases at a selective circadian time to allow time-dependent activation of intracellular cyclic AMP signalling in the SCN. Gene ablation of *Rgs16* leads to the loss of circadian production of cAMP and as a result lengthens circadian period of behavioural rhythm. The temporally precise regulation of the cAMP signal by clock-controlled RGS16 is needed for the dorsomedial SCN to maintain a normal phase-relationship to the ventrolateral SCN. Thus, RGS16-dependent temporal regulation of intracellular G protein signalling coordinates the intercellular synchrony of SCN pacemaker neurons and thereby defines the 24 h rhythm in behaviour.

[1] Department of Systems Biology, Graduate School of Pharmaceutical Sciences, Kyoto University, Kyoto 606-8501, Japan. [2] Division of Molecular Brain Science, Graduate School of Medicine, Kobe University, Kobe 650-0017, Japan. [3] Department of Genomic Drug Discovery Science, Graduate School of Pharmaceutical Sciences, Kyoto University, Kyoto 606-8501, Japan. [4] Division of Advanced Sciences, Ochadai Academic Production, Ochanomizu University, Tokyo 112-8610, Japan. [5] PRESTO, Japan Science and Technology Agency, Kawaguchi 332-0012, Japan. [6] Education Unit for Global Leaders, Kyoto University, Kyoto 606-8501, Japan. [7] Laboratory for Animal Resources and Genetic Engineering, Riken Center for Developmental Biology, Kobe 650-0047, Japan. [8] Department of Electronics, Tohoku Institute of Technology, Sendai 982-8577, Japan. [9] Department of Neuroscience, The Ohio State University, Ohio 43210, USA. *These authors contributed equally to this work. Correspondence and requests for materials should be addressed to H.O. (email: okamurah@pharm.kyoto-u.ac.jp).

In mammals, the hypothalamic suprachiasmatic nucleus (SCN) is a central pacemaker, governing daily rhythms in behaviour and physiology[1–3]. Individual neurons in the SCN act as cell-autonomous oscillators, exhibiting circadian fluctuations of firing rate and gene expression[4–7]. We and others have recently shown that autonomous SCN neuronal oscillators maintain a high degree of synchrony with each other, so that they can generate coherent signals required for the circadian control of behaviour and physiology[6–10].

While individual SCN neurons share the same circadian period as a result of synchronization, the phases of their rhythms are strikingly diverse[6]. This observation reflects the reality that the SCN is an anatomically heterologous cellular assemblage, in which cohorts of differentially phased cellular clocks are deployed in a topographically specific manner[11,12]: neurons in the dorsomedial part of the SCN reach their daily peak in clock gene expression earlier in the day than those in the rest of the SCN. However, the mechanism by which dorsomedial SCN cells maintain their relatively advanced phasing, and to what extent this differential phasing influences the rhythms in behaviour have remained unknown.

Much better understood is the molecular mechanism underlying cell-autonomous circadian oscillations. These rely on the opposing effects of transcriptional activators and repressors that generate negative feedback loops[13–15]. Briefly, the transcriptional activators CLOCK and BMAL1 drive transcription of *Period* (*Per1* and *Per2*) and *Cryptochrome* (*Cry1* and *Cry2*) genes via binding to E-box elements present in their promoters. Once the repressor proteins PER and CRY reach a critical concentration, they form complexes and repress their own expression by inhibiting the CLOCK/BMAL1 complexes. In addition to E-box elements, the promoter regions of *Per* genes contain D-boxes, through which the PAR bZip family of transcriptional activators (DBP, TEF and HLF) and the related repressor E4BP4 exert their opposing effects on the expression of target genes[16–20]. Finely controlled transcriptional regulation through the E-box and D-box motifs is thought to generate robust circadian expression of *Per* genes as well as a wide variety of clock-controlled genes[21].

Although cell-autonomous transcriptional regulation of clock genes could provide a common mechanism underlying the oscillations of individual cells, this does not explain the phasic differences between the neurons in the SCN. In this regard, it is important to note that the promoter region of *Per1* gene contains a functional cyclic AMP-responsive element[22], and that the extracellular signalling that activates cAMP pathway can acutely induce *Per1* expression[23]. Because a light pulse given in the night time induces *Per1* expression in the SCN, this pathway has long been considered crucial for light-dependent resetting of the phase of the molecular clock[24–26]. Yet, the cAMP-dependent control of *Per1* may also have a role in coordinating circadian rhythms (phase-arrangement) of neurons in the SCN[14]. Supporting this hypothesis, the concentration of cAMP and transcriptional activity of the cAMP-responsive element in the SCN are both highly rhythmic even in constant darkness[27–29]. Moreover, pharmacological reduction in the rate of cAMP synthesis in the SCN lengthens the circadian period of the behavioural rhythm[29], demonstrating a role of cAMP in the determination of the circadian period.

RGS16 is a potential regulator of rhythmic cAMP synthesis in the SCN. Biochemically, RGS16 functions as a GTPase-accelerating protein for Gαi/o subtypes of G protein α subunits[30–32]. By promoting GTP hydrolysis, RGS16 terminates GTP-bound (thus activated) Gαi/o signalling. Microarray studies and the subsequent expression analyses revealed that the gene encoding RGS16 exhibits circadian variations in the levels of transcript in the SCN[33–36]. These data raise the possibility that Gαi/o-mediated cAMP signalling in the SCN is under circadian regulation via RGS16.

Here we show that gene ablation of *Rgs16* leads to the loss of circadian production of cAMP in the SCN, which results in a period lengthening of the locomotor activity rhythm. Extensive analysis of the intercellular phase-relationship within the SCN reveals that the RGS16-mediated daily activation of cAMP is necessary to accelerate the expression of *Per1* in the dorsomedial cells. Our data therefore demonstrate that RGS16-mediated cAMP signalling defines the advanced phasing of dorsomedial cells, and as such, is a critical determinant for the period of circadian rhythms in behaviour.

Results

Gene expression profiles of the RGS family in the SCN. It is known that pharmacological inhibition of Gαi/o activity with pertussis toxin hampers intercellular synchronization[37] and causes dampened rhythms of the entire SCN (Supplementary Fig. S1)[37]. These observations prompted us to hypothesize that member(s) of the regulator of G protein signalling (RGS) family might contribute to synchronized cellular oscillations in the SCN. We surveyed all known mouse *Rgs* genes for their expression in the SCN by using DNA microarray analysis (Supplementary Fig. S2a). Then, the genes highly expressed in the SCN were selected and further analysed with quantitative *in situ* hybridization to specify their histological distribution and circadian time (CT)-dependent expression profile (Supplementary Fig. S2b)[38]. This survey led us to notice that *Rgs16* is the only RGS family member that displays marked SCN-specific expression particularly in the subjective daytime (see CT4 in Fig. 1a; CT4 corresponds to 4 h after subjective onset of daytime under constant dark conditions). This expression profile, together with a prior work showing that RGS16 regulates Gαi/o activity[31,32], raised the prospect that RGS16 contributes to SCN circadian clock physiology.

Cyclic expression of *Rgs16* is driven by the circadian clock. Time-dependent profiling revealed that *Rgs16* exhibits overt circadian expression in the SCN (Fig. 1b), which persists even in constant darkness (DD) with a drastic increase of expression in the early subjective morning. Topographical analysis by digoxigenin *in situ* hybridization (Fig. 1c) further demonstrated that *Rgs16* expression began to increase by subjective dawn (CT0) in the periventricular part of the dorsomedial SCN (a narrow but cell-dense area near the third ventricle). Thereafter, *Rgs16*-positive staining spread widely across the SCN at CT4. At CT8, *Rgs16* levels began to decrease in all SCN regions, and throughout the subjective night (that is, CT12–20) expression was limited to a few SCN cells. The spatiotemporal expression of *Rgs16* resembles that of *Per1*, a clock gene showing peak messenger RNA expression during the daytime in the SCN[11,12]. Similar to the *Per1* promoter, the 5′-flanking genomic sequence of *Rgs16* contains E-box and D-box *cis*-regulatory elements, thus allowing the circadian regulators CLOCK–BMAL1 and DBP to activate transcription. In a further parallel with *Per1*, CRY1 and E4BP4 repressed CLOCK–BMAL1- and DBP-evoked *Rgs16* expression, respectively (Supplementary Figs. S3 and S4). Consistent with the promoter characteristics, *in vivo* circadian expression of *Rgs16* was dramatically altered in the PAR bZip proteins-deficient mice ($Dbp^{-/-}$ $Tef^{-/-}$ $Hlf^{-/-}$)[39] as well as *Clock* mutant and $Cry1^{-/-}$ $Cry2^{-/-}$ mice (Supplementary Fig. S4f). In *Clock* mutant mice, the early subjective day peak in *Rgs16* expression was damped whereas in $Cry1^{-/-}Cry2^{-/-}$ mice *Rgs16* expression was high at both the subjective day and night time points. These data clearly demonstrate that expression of *Rgs16* is under the control of the intracellular clock machinery. It is also noteworthy that the expression of *Rgs16* was not light-inducible (Supplementary Fig. S5). Thus, the internal clock seems to drive the morning expression of *Rgs16* in the SCN.

RGS16 deficiency lengthens the circadian period of behaviour. To characterize the *in vivo* function of RGS16, we generated RGS16-deficient mice, in which a genomic region spanning whole coding sequence of *Rgs16* was deleted and replaced with a lacZ reporter cassette (Fig. 1d,e). *In situ* hybridization analysis (Fig. 1f) con-

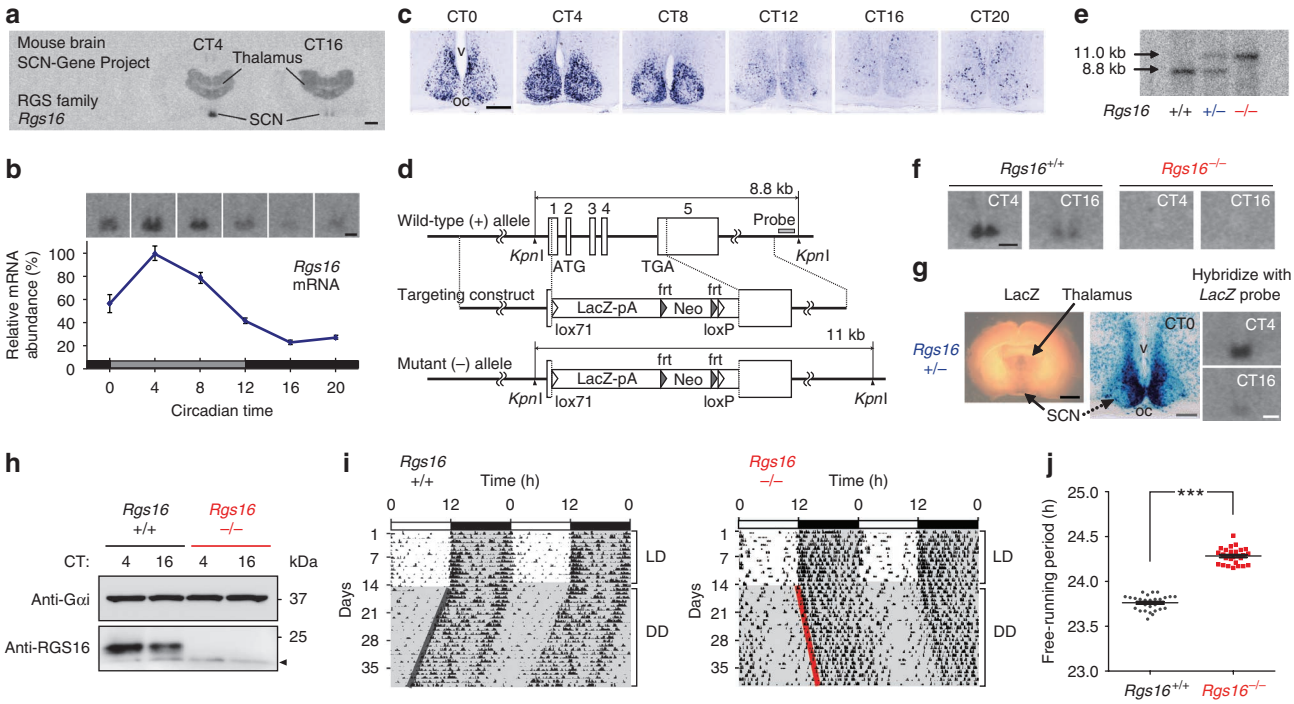

Figure 1 | RGS16 deficiency lengthens the circadian period of the locomotor activity rhythm. (**a**) Autoradiographs showing mouse coronal brain sections hybridized with an *Rgs16* probe. CT4 and CT16 correspond respectively to 4 and 16 h after the subjective onset of daytime in DD. Bar, 1 mm. (**b**) Circadian expression of *Rgs16* in the SCN in DD. Relative RNA abundance was quantified with radioisotopic *in situ* hybridization. Values means ± s.e.m ($n = 5$) with the peak value adjusted to 100. Representative autoradiographs at the indicated time points are shown on the top. Bar, 200 µm. (**c**) Digoxigenin *in situ* hybridization showing the distribution of *Rgs16*-positive cells in the SCN. oc, optic chiasm; v, third ventricle. Bar, 100 µm. (**d**) Schematic representation of the mouse *Rgs16* gene, targeting construct, and the mutant allele. Numbered boxes are the exons. The DNA probe used for southern blots is marked by a grey box. (**e**) Southern blot of *Kpn*I-digested DNA from *Rgs16*$^{+/+}$, *Rgs16*$^{+/-}$ and *Rgs16*$^{-/-}$ mice, WT (8.8 kb) and mutant (11 kb) allele. (**f**) Radioisotopic *in situ* hybridization autoradiographs showing WT and *Rgs16*$^{-/-}$ SCN. Bar, 200 µm. (**g**) *Rgs16*$^{+/-}$ coronal brain slice stained with X-gal (blue) with a magnified view of the SCN in a thin brain section at CT0. Autoradiographs show quantitative *LacZ* mRNA *in situ* hybridization at CT4 and CT16. Scale bars: black, 1 mm, grey, 100 µm, white, 300 µm. (**h**) Western blots of RGS16 and Gαi in the SCN at CT4 and CT16. Arrowhead indicates a non-specific band. (**i**) Representative locomotor activity records of C57BL/6J-backcrossed *Rgs16*$^{+/+}$ and *Rgs16*$^{-/-}$ mice. Mice were housed in a 12L:12D light–dark cycle and then transferred to DD. Periods of darkness are indicated by grey backgrounds. The data are shown in double-plotted format. Each horizontal line represents 48 h; the second 24-h period is plotted to the right and below the first. The coloured lines delineate the phase of activity onset in DD. (**j**) Period-length distribution of C57BL/6J-backcrossed *Rgs16*$^{+/+}$ and *Rgs16*$^{-/-}$ mice. Free-running period measurements were based on a 14-day interval taken after 3 days of a DD regime and were executed with a χ^2 periodogram. Plotted are the period lengths of individual animals. Bars indicate mean ± s.e.m. ***$P < 0.001$, Student's *t*-test.

firmed the loss of the *Rgs16* transcript in *Rgs16* homozygous mutant (*Rgs16*$^{-/-}$) mice. β-galactosidase tissue staining (Fig. 1g) further corroborated gene targeting and replacement by *LacZ*: the spatio-temporal expression of the transgene reflected *Rgs16* expression in the SCN. Moreover, we generated an antibody to RGS16 and performed immunoblot analysis with SCN extracts (Fig. 1h). As expected, the expression of RGS16 was not detected in *Rgs16*$^{-/-}$ mice, whereas wild-type (WT) mice exhibited an increased expression of RGS16 protein in the subjective morning (Fig. 1h). We thus conclude that *Rgs16* mutant mice are indeed RGS16-deficient.

Behavioural analysis was performed with *Rgs16* mutant mice that had been backcrossed to the C57BL/6J background over ten generations. We observed that the gene ablation of *Rgs16* causes a lengthening of circadian period of the locomotor activity rhythm (Fig. 1i): under constant darkness, all *Rgs16*$^{-/-}$ mice tested ($n = 27$) showed a free-running period longer than 24 h (circadian period (mean ± s.e.m) determined with a χ^2 periodogram, 24.28 ± 0.01 h). The phenotype of *Rgs16* knockout sharply contrasts with that of *Rgs16*$^{+/+}$ control mice ($n = 29$), whose period is shorter than 24 h (23.76 ± 0.01 h). The difference between the two genotypes is statistically significant (Fig. 1j, $P < 0.001$, Student's *t*-test) and does not depend on the way of measuring circadian period (periods determined with a linear regression line method: *Rgs16*$^{+/+}$, 23.77 ± 0.01 h; *Rgs16*$^{-/-}$, 24.31 ± 0.01 h, $P < 0.001$, Student's *t*-test), revealing that *Rgs16* is a critical determinant of the behavioural rhythm period length. In contrast to the altered circadian periodicity under constant darkness, *Rgs16*$^{-/-}$ mice displayed a normal 24 h rhythm when maintained in 12-h-light/12-h-dark cycle (Fig. 1i) and their resetting response to early and late night light pulses were indistinguishable from WT mice (Supplementary Fig. S6). Thus, RGS16 is not necessary for light entrainment of the circadian clock. Rather, signalling through RGS16 comprises a pathway responsible for the maintenance of the normal circadian rhythm.

RGS16 targets Gαi and regulates cAMP production in the SCN. RGS16 is known to negatively regulate Gαi proteins, which downregulate cAMP production by inhibiting adenylate cyclase (AC) activity[31,32]. Double *in situ* hybridization revealed that both *Gnai1* mRNA and *Gnai2* mRNA (encoding Gαi1 and Gαi2, respectively) colocalize with *Rgs16* in SCN neurons (Fig. 2a). Intriguingly, whereas the levels of Gαi1 and Gαi2 proteins were nearly constant throughout the day, the amount of RGS16 protein in the SCN showed overt circadian oscillation (Fig. 2b). Consistent with the GTPase-accelerating protein activity of RGS16, protein pull-

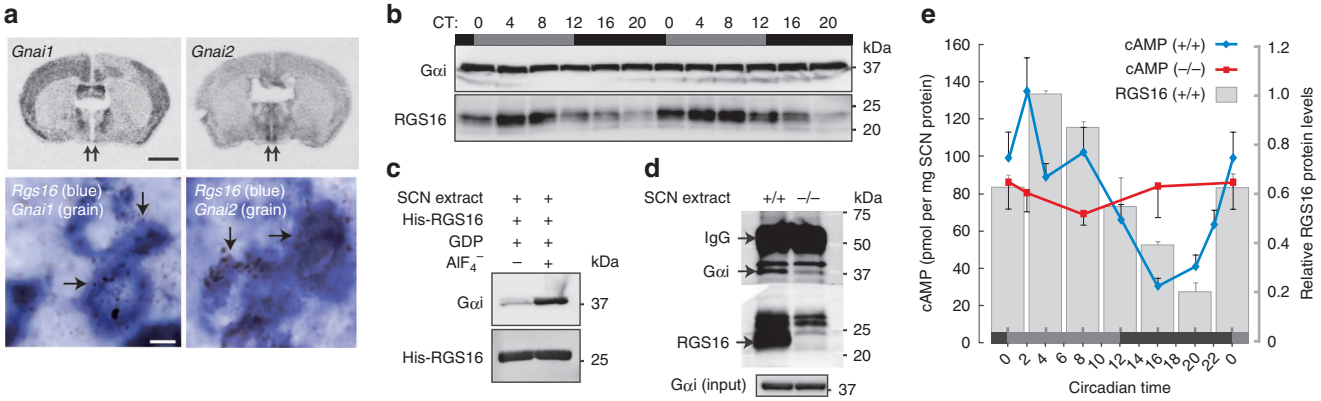

Figure 2 | RGS16 protein targets Gαi and regulates circadian production of cAMP in the SCN. (**a**) (Upper) Low-power film autoradiography showing the mouse coronal brain sections *in situ* hybridized with radioisotopic probe for *Gnai1* or *Gnai2*. Arrows indicate the positions of the SCN. Bar, 2 mm. (Lower) High-power photomicrographs of the SCN double *in situ* hybridized with digoxigenin-labelled probe for *Rgs16* (*blue*) and isotope-labelled probe for *Gnai1* or *Gnai2* (*silver grains*). Arrows indicate representative double-labelled cells. Bar, 5 μm. (**b**) Western blots analysing the temporal changes in the protein levels of RGS16 and Gαi in the WT mouse SCN. The animals kept in DD were killed at 4-h intervals across two circadian cycles (sampling times indicated at the top). The microdissected SCN extracts were probed with antibodies to RGS16 and Gαi. The Gαi antibody used recognizes both Gαi1 and Gαi2. (**c**) Increased binding affinity of RGS16 and Gαi in aluminium fluoride-treated SCN extracts. The microdissected SCN extract was incubated with His-tagged RGS16 protein in the presence of GDP with or without aluminium fluoride. Shown are Western blots of the proteins affinity purified with Ni-NTA beads. (**d**) Immunoprecipitation (IP) of endogenous Gαi with endogenous RGS16. The microdissected SCN extracts from *Rgs16*$^{+/+}$ or *Rgs16*$^{-/-}$ mice at CT0 (input) were subjected to IP with RGS16 antibody. Shown are Western blots of the immunoprecipited RGS16 and Gαi (upper) and input Gαi (lower). (**e**) Circadian changes of cAMP content in the microdissected SCN from *Rgs16*$^{+/+}$ (blue) and *Rgs16*$^{-/-}$ (red) mice (means ± s.e.m, $n = 10$, for each time point). $P < 0.01$, CT2 (peak) versus CT16 (trough) in *Rgs16*$^{+/+}$ mice. Such a temporal difference is not detected in *Rgs16*$^{-/-}$ mice. To characterize more precisely the cAMP rhythm seen in WT mice, cAMP contents in the WT SCN were determined at shorter sampling intervals. The bar graph shows the levels of RGS16 protein in the SCN (means ± range of variation) assessed from the results in **b** by densitometric analysis.

down assays demonstrated that Gαi proteins in the SCN displayed an increased binding affinity for RGS16 when SCN extracts were treated with aluminium fluoride (AlF_4^-–GDP complex forms a transition state analogue of GTP hydrolysis) (Fig. 2c). Furthermore, immunoprecipitation of endogenous RGS16 protein at CT0 showed that the Gαi proteins coprecipitated with RGS16 from the protein extract of the WT SCN, but not from that of the *Rgs16*$^{-/-}$ SCN (Fig. 2d).

Time-of-day specific inhibition of Gαi by RGS16 might affect circadian production of cAMP in the SCN, which has recently been proved crucial for the maintenance of robust circadian oscillations[29]. Consistent with this model, we found that cAMP concentrations in the WT SCN fluctuated in a circadian fashion, rising synchronously with the expression of RGS16 in the subjective morning (Fig. 2e). Furthermore, we observed that the circadian fluctuation of cAMP was abolished as a result of RGS16 deletion (Fig. 2e). Interestingly, in *Rgs16*$^{-/-}$ mice, cAMP was maintained at intermediate levels throughout the day, implying that compensatory processes augment cAMP production. Hence, our data indicate that RGS16 is indispensable for conferring circadian rhythmicity (that is, time-of-day specificity) on the production of cAMP in the SCN.

Delayed *Per1* cycling in RGS16-deficient dorsomedial cells. The *Per1* gene is a central clock component that is linked to cAMP signalling through a cAMP-responsive element within its promoter region[22] (Supplementary Fig. S3). Therefore, we examined the integrity of *Per1* expression in the *Rgs16*$^{-/-}$ SCN (Fig. 3). Although circadian expression of *Per1* in the mutant SCN was grossly normal, close inspection with digoxigenin *in situ* hybridization led us to identify a defect of *Per1* expression in a small subset of cells located in the periventricular part of the dorsomedial SCN (Fig. 3a). Intriguingly, this region is anatomically characterized by a cluster of 'phase-leading' cells[11,12] in which *Per1* mRNA levels peak at the beginning of the day, preceding the *Per1* mRNA peak in ventral SCN cells. We observed that in *Rgs16*$^{-/-}$ SCN, the rising phase of *Per1* mRNA expression in the periventricular part of the dorsomedial SCN is significantly delayed, relative to that of WT SCN (Fig. 3a and detailed profiles of *Per1* expression in Supplementary Figs. S7 and S8). Thus, we speculated that cAMP signalling through RSG16 might be crucial for the phase-advanced expression of *Per1* at dawn in the dorsomedially located phase-leading cells.

To complement these observations, we analysed the *Per1* expression profile in organotypic brain slices from *Per1* promoter-luciferase (*Per1-luc*) transgenic mice[6] (Fig. 3b-f). Real-time bioluminescence imaging with high-resolution video microscopy[6] allows us to monitor the circadian dynamics of hundreds of individual neurons in morphologically preserved SCN slices[40], where the luminescence driven by the *Per1* promoter recapitulates the topographic- and time-dependent expression of *Per1* mRNA (Fig. 3b–f, Supplementary Fig. S9 and Supplementary Movie 1, *Per1-luc Rgs16*$^{+/+}$ SCN). Thus, the phase-advanced oscillation, observable *ex vivo* in WT dorsomedial cells (Fig. 3b–f) is a property inherent to the SCN[6]. Taking advantage of this system, we examined *Per1-luc* rhythms in SCN slices from *Rgs16*$^{-/-}$ mice (Fig. 3b–f, Supplementary Fig. S9 and Supplementary Movie 1, *Per1-luc Rgs16*$^{-/-}$ SCN). In line with *in vivo* data from *Rgs16*$^{-/-}$ mice, the luminescence of the *Rgs16*$^{-/-}$ SCN slice was basically circadian, and its period was relatively long compared with that of WT slice (circadian period (h), mean ± s.e.m., *Rgs16*$^{+/+}$, 24.35 ± 0.03; *Rgs16*$^{-/-}$, 24.82 ± 0.07, $n = 6$ for each genotype, $P < 0.05$, *t*-test). Furthermore, when the phase differences across three SCN zones (dorsal, middle and ventral) were examined, the dorsal zone, which includes phase-leading cells, exhibited a delayed (relative to *Rgs16*$^{+/+}$) circadian oscillation, with a resultant phase close to that of the remaining zones (Fig. 3d and Supplementary Fig. S9b). Importantly, such alteration of dorsal rhythm was observed in all *Rgs16*$^{-/-}$ SCN slice cultures tested, and statistical analysis revealed that the luminescence from the dorsal zone of the *Rgs16*$^{-/-}$ SCN reached its peak at a time significantly later than that of the *Rgs16*$^{+/+}$ SCN (Fig. 3e and Supplementary Fig. S9c).

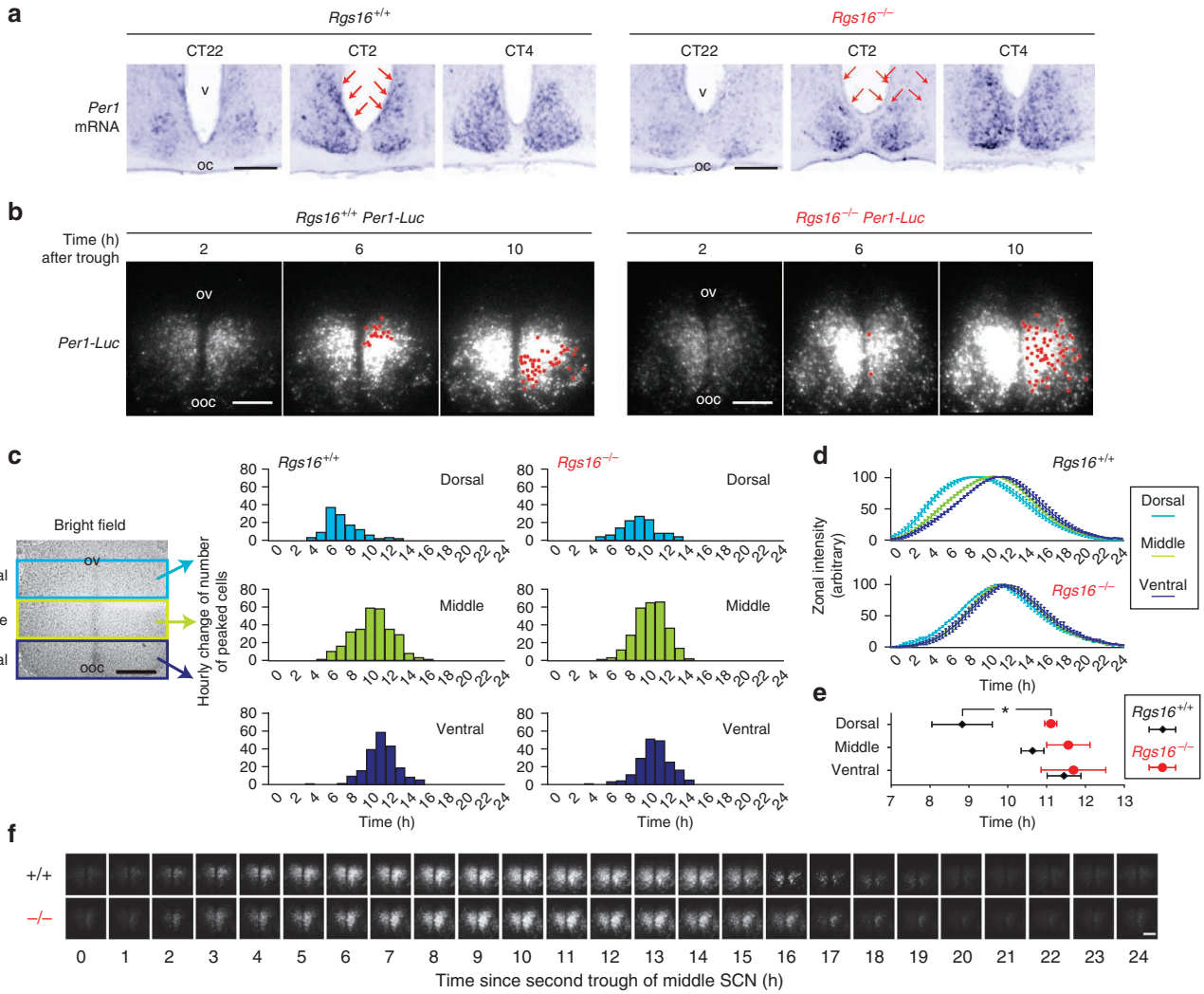

Figure 3 | RGS16 deficiency impairs *Per1* expression in dorsomedially located phase-leading cells. (**a**) Digoxigenin *in situ* hybridization photomicrographs showing the topographical distributions of *Per1*-positive cells in the SCN at CT22, CT2 and CT4. (**b**) Bioluminescent images of whole SCN slices from *Per1-luc* -bearing *Rgs16*$^{+/+}$ and *Rgs16*$^{-/-}$ mice. The red spots on the right-side nucleus indicate the positions of the peaked cells at the indicated time point after the trough of the total SCN bioluminescence. (**c**) The range of peak times of randomly chosen cells from the subdivided dorsal (n = 116, for each genotype), middle (n = 281) and ventral (n = 193) SCN zones of WT and mutant slices. For non-biased definition of the regions of interest, the SCN was divided into three regions with equal proportions along vertical axis (from the dorsal-most to the ventral-most). The x axis represents time (h) since 2nd trough of middle SCN luminescence. Note that the region selected as a dorsal zone encompasses the phase-leading cells. (**d**) The temporal changes in the levels of total luminescence from each zone (means ± s.e.m (n = 4); the peak and trough values were adjusted to 100 and 0, respectively). Two-way ANOVA with repeated measures identify a statistically significant interaction between zone and genotype ($F(2,18) = 6.88$, $P < 0.001$). Bonferroni's *post hoc* tests reveal statistically significant difference between WT and *Rgs16*$^{-/-}$ slices only in dorsal zone, but not in middle and ventral zones. (**e**) The average times of peaks (± s.d.) from subdivided dorsal, middle and ventral SCN zones of WT and mutant slices (n = 4, for each genotype). *P < 0.001 (Bonferroni test). (**f**) Hourly images of the SCN slices from *Rgs16*$^{+/+}$ and *Rgs16*$^{-/-}$ mice. See also Supplementary Movie 1. Scale bars in (**a**–**f**) are 100 μm. v, third ventricle; ov, original third ventricle; oc, optic chiasm; ooc, original optic chiasm.

Impaired cAMP signalling in RGS16-deficient dorsomedial cells. The observations thus far indicate that dorsomedial SCN cells are the major (or sole) site where the RGS16-cAMP pathway could contribute to the rising phase of the *Per1* mRNA. Consistent with this finding, we observed that the dawn expression of *Per1* in the dorsomedial cells was unique in that it accompanied a strong induction of *cFos* (Fig. 4a and Supplementary Fig. S10)[41,42]. as well as a simultaneous activation of extracellular signal-regulated kinase (ERK) (Fig. 4b and Supplementary Fig. S10)[43–45]. Of note, both of these events were cAMP-dependent (Fig. 4c–e); hence, the pharmacological inhibition of cAMP synthesis *in vivo* with 9-(tetrahydro-2-furyl)-adenine (THFA, a noncompetitive AC inhibitor, which slows the rate of cAMP production but does not completely deplete cAMP[29]) suppressed the dawn induction of *cFos* and phospho-ERK that otherwise appeared in the periventricular part of the dorsomedial SCN (Fig. 4c–e and Supplementary Fig. S10). Thus, the activated cAMP pathway at dawn is a feature characterizing the phase-leading cells.

Importantly, the dorsomedial cell-specific induction of *cFos* and ERK phosphorylation at dawn were both severely compromised by RGS16 deficiency (Fig. 4a,b), demonstrating that RGS16 determines the state of cAMP-dependent signalling in the phase-leading cells. We also observed that the animals treated with THFA phenocopied *Rgs16*$^{-/-}$ mice (Figs. 1i and 4c), displaying a relatively long circadian locomotor activity rhythm (Figs. 1j and 4f). Thus, we concluded that cAMP signalling at dawn in the phase-leading cells depends on RGS16, and that the loss of RGS16-cAMP signalling causes a

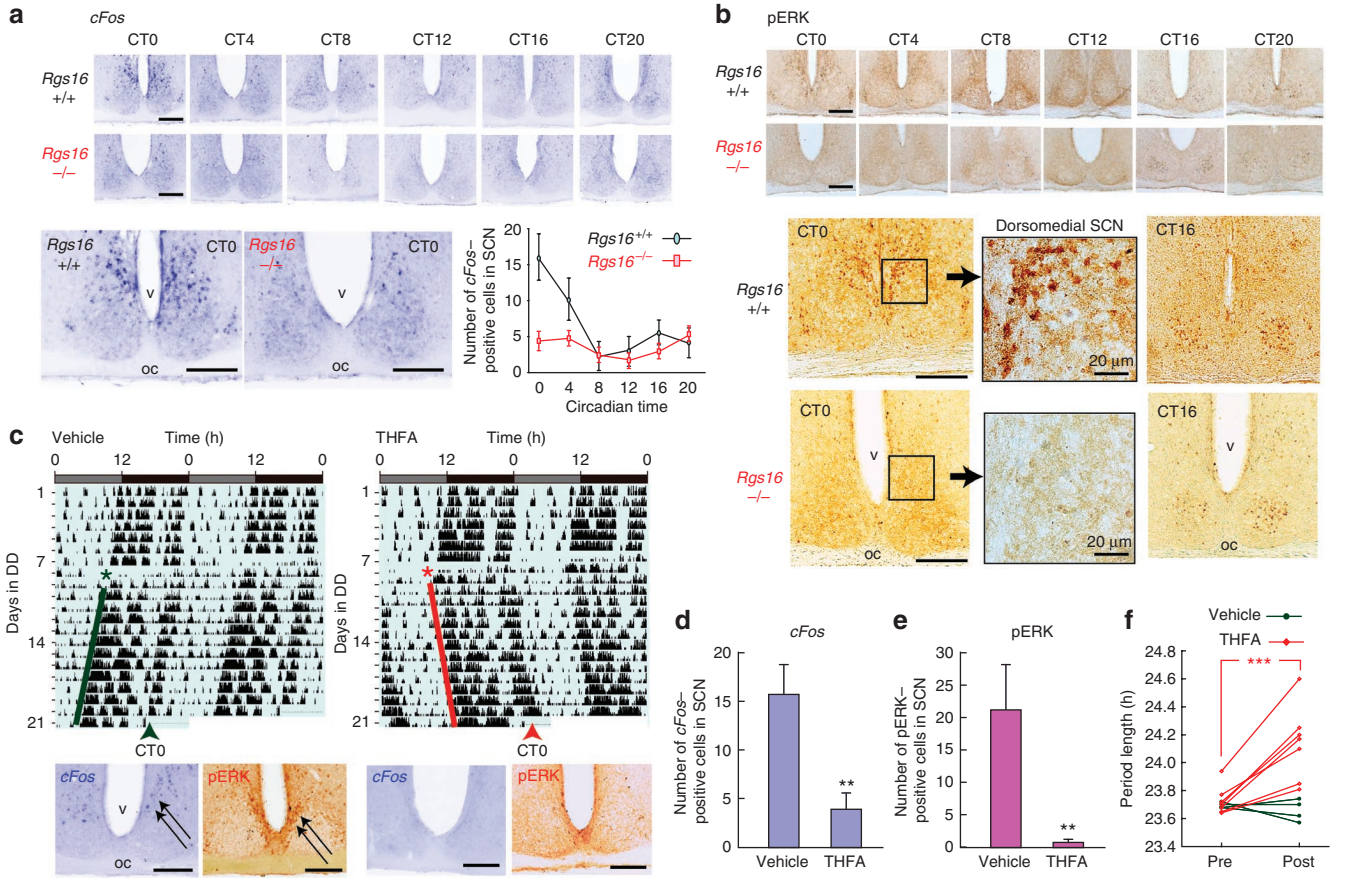

Figure 4 | RGS16 deficiency impairs cAMP-dependent induction of *cFos* and ERK phosphorylation. (**a**) Digoxigenin *in situ* hybridization photomicrographs showing the circadian profiles of *cFos* expression in the SCN of *Rgs16*$^{+/+}$ and *Rgs16*$^{-/-}$ mice under DD conditions. The graph indicates the number of *cFos*-positive cells (per section) across the circadian time (means ± s.e.m, $n = 5$). (**b**) Immunoreactivity to the pERK in the SCN of *Rgs16*$^{+/+}$ and *Rgs16*$^{-/-}$ mice under DD conditions. (**c**) Representative locomotor activity records of WT mice under DD conditions before and after the surgery (asterisk) for the continuous infusion of THFA or vehicle (delivered to third ventricle just upper to the SCN via osmotic minipump). Arrowheads indicate the day on which the mice were killed at CT0 (estimated by the phase of the activity onset) for the analysis of *cFos* and pERK expression in the SCN. Representative photomicrographs are shown below the locomotor activity records. Scale bars in **a**–**c** are 100 μm unless otherwise noted. (**d**, **e**) The histograms showing the number (means ± s.e.m) of *cFos*- (**d**) or pERK- (**e**) positive cells in the SCN (per section) at CT0 after 14-days infusion of either THFA ($n = 6$) or vehicle ($n = 6$) in DD. $^{**}P < 0.01$, *t*-test, compared with vehicle treatments. (**f**) Pair-wised comparisons of behavioural periods before and after infusion of THFA ($n = 6$) or vehicle ($n = 4$). $^{***}P < 0.001$, paired *t*-test in THFA-treated mice. pERK, phosphorylated form of ERK.

lengthening of the circadian period (or a constantly delayed phase) of the locomotor activity rhythm of mice.

Discussion

A critical issue for understanding SCN function is to identify how individual cellular clocks synchronize with a defined intercellular phase-relationship to broadcast coherent circadian signals to peripheral tissues and thereby coordinate physiology and behaviour. We previously showed that the dorsomedial SCN cells run ahead of the remaining cells, and that this differential phasing is an intrinsic property arising from the intercellular network of the SCN. However, the molecular mechanism underlying the phase-advanced oscillations of the dorsomedial cells and how they contribute to behavioural rhythms have remained unknown. In the present study, we have shown that the induction of dorsomedial *Per1* expression at dawn is constantly accelerated by the circadian activation of intracellular cAMP signalling, which requires coordinated inhibition of Gαi by the clock-controlled RGS16 (see a schematic model in Fig. 5). Importantly, RGS16 deficiency, which delays dorsomedial *Per1* expression, results in a period lengthening of behavioural rhythm. These data therefore reveal that the temporal regulation of intracellular G protein signalling that dictates the phasic arrangement within the SCN contributes to the determination of the circadian period of locomotor activity rhythm.

We found that despite the disappearance of the cAMP rhythm, *Rgs16*$^{-/-}$ mice still show *Per1* oscillations in the SCN (Fig. 3). This observation may be somewhat unexpected because pharmacological depletion of cAMP by an irreversible potent AC inhibitor (MDL-12,330A) constitutively reduces *Per1* expression to basal levels[29]. It should be noted, however, that the concentrations of cAMP in the *Rgs16*$^{-/-}$ SCN (Fig. 2e) and in THFA (a mild AC inhibitor)-treated cells[29] were not markedly reduced (kept at intermediate levels), and that under these conditions behavioural rhythms were sustainable, albeit with a relatively long circadian period (Figs. 1i and 4c)[14]. Consistent with this behavioural rhythm, the circadian fluctuations of *Per1* in the *Rgs16*$^{-/-}$ SCN were mostly unimpaired: rhythms in the vast majority of middle-to-ventral cells remained intact, and intriguingly, even in the dorsomedial cells, *Per1* was still capable of oscillating, albeit with its peak phase significantly delayed due to RGS16 deficiency (Fig. 3d,e). Thus, the oscillations of *Per1* in the SCN are not necessarily depending on the cAMP rhythm, but are rather self-sustainable, presumably due to transcriptional control through E-box and D-box, which might suffice to drive 'normal' (that is, non-phase-leading) *Per1* expression. Our data therefore

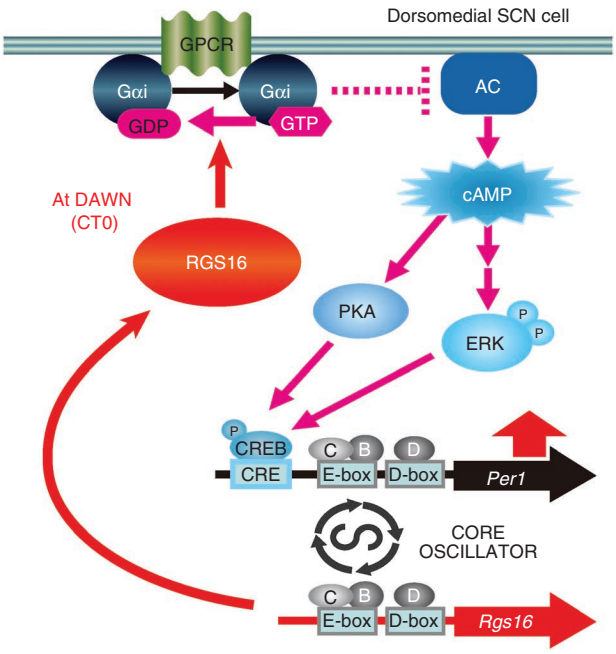

Figure 5 | Schematic model depicting a role of RGS16 in regulated cAMP signalling at dawn in the dorsomedial cells. Through allowing cAMP synthesis at dawn, RGS16 regulates *Per1* expression in the dorsomedial phase-leading cells. B, BMAL1; C, CLOCK; CRE, cAMP responsive element; CREB, CRE-binding protein; D, DBP; P, phosphate; ERK, extracellular signal-regulated kinase; PKA, cAMP-dependent protein kinase.

propose that the major role of the daily activation of cAMP in the SCN is to accelerate the expression of *Per1* in the dorsomedial cells, thereby advancing the phases of these cells, relative to those of the cells in the middle-to-ventral SCN.

RGS16 is an inhibitor of Gαi. How Gαi is activated in the SCN remains unknown. Gαi could be activated by extracellular or intracellular signals. One candidate, Dexras1, is a nonreceptor-associated activator for Gαi[46]. Interestingly, the gene encoding Dexras1 is highly and rhythmically expressed in the SCN, with a phase almost anti-phasic to that of *Rgs16*, and mice lacking Dexras1 show abnormal desynchronization of the behavioural rhythm in constant light[47]. These results raise the prospect that the temporally segregated activation and inhibition of Gαi by Dexras1 and RGS16 might contribute to circadian control of Gαi. Besides Dexras1, Gαi-coupled GPCR signalling may also be involved. Defining which specific Gαi activators are required for SCN synchrony and how they act in concert with RGS16 will be our next challenge. It is also noteworthy that pharmacological (global) silencing of Gαi/o with pertussis toxin treatment could dampen SCN rhythm[37], a phenotype differing from that of RGS16 deficiency. Thus, the mechanism(s) by which pertussis toxin affects SCN physiology remains unknown. We should also mention that RGS16 can target Gαq[30]. Given that in multiple cell types, Gαq-mediated Ca^{2+} signalling interferes with cAMP production[48–50], it will be worth testing whether Gαq signalling in the SCN is subject to the circadian regulation by RGS16 and how this potential pathway contributes to the altered cAMP signals in the RGS16-deficient SCN.

In line with previous reports, we observed that the expression of *cFos* at dawn in the SCN is highly confined to the dorsomedial cells (Fig. 4a)[41,42]. This spatially limited activation of *cFos* cannot be explained by RGS16 distribution (Fig. 1c): *cFos* expression does not parallel the expression of *Rgs16* in middle-to-ventral SCN regions, making it unlikely that RGS16 expression by itself suffices to drive *cFos* induction. Rather, given that the role of RGS16 is to inhibit Gαi and temporarily permit the production of cAMP in the SCN, it would be reasonable to speculate that RGS16 is necessary (Fig. 4a) but not sufficient to drive cAMP synthesis that triggers the expression of *cFos* in the dorsomedial cells. It is conceivable that the circadian regulation of cAMP is a multifactorial process involving not only Gαi but also Gαs. Along these lines, the vasoactive intestinal peptide, a neurotransmitter mediating cell–cell communication in the SCN, activates Gαs by acting through its cognate receptor $VPAC_2$[8,9,51]. As it has been speculated that vasoactive intestinal peptide acts on the dorsomedial SCN[52], further investigations aimed at deciphering the rules governing the precisely timed and topologically specific activation of Gαs and Gαi pathways in the SCN will be required to understand how cAMP synthesis in the SCN is controlled.

Because the lengthened period of the *Rgs16*$^{-/-}$ behavioural rhythm (Fig. 1i,j) is closely associated with the delayed phase of the periventricular part of the dorsomedial SCN (Fig. 3a and Supplementary Figs. S7 and S8), we envisage that the functional changes in a small subset of neurons (for example, phase-leading cells) could alter the global timing property of the SCN. We observed that this prediction is mathematically feasible at least in a two-coupled cell-oscillator model that we constructed *in silico* (Supplementary Fig. S11). The mathematical configuration used was based on a published model which hypothesizes a mutual coupling between the two oscillators[53,54] and was modified by introducing a term accounting for the dawn cAMP signal in a phase-leading cell (see Supplementary Methods for details). Under these conditions, the cell oscillating *in silico* with cAMP signalling at dawn runs ahead of the cell without cAMP signalling, and both cells exhibit the same circadian period (23.6 h) (see Supplementary Fig. S11). By contrast, once cAMP signalling was deleted from the phase-leading cell, then the two cells began to oscillate in phase with an elongated circadian period (24.4 h) (Supplementary Fig. S11), a situation similar to what was observed for *Rgs16*$^{-/-}$ mice under constant dark conditions. Thus, a modified two-coupled cell-oscillator model predicts the period lengthening by delayed circadian oscillation of phase-leading cells, whereas further elucidation of SCN network will be needed to faithfully recapitulate whole SCN function (see Supplementary Methods for detailed discussion).

In conclusion, we provide evidence that RGS16, known as the regulator of *intra*cellular Gαi protein signalling, is a key component to establish the *inter*cellular phase-relationship of multi-phased SCN neurons. Mechanistically, RGS16 forms an integration point whereby the intracellular molecular clock exerts its effect on cAMP signalling (Fig. 5). Through allowing cAMP synthesis at dawn, RGS16 in turn facilitates the phase-advanced expression of *Per1* in the dorsomedial cells. Thus, our work adds a new layer of complexity to the rules that govern the intercellular synchrony of SCN neurons. We propose that signalling at the cell surface is not everything. Rather, the circadian time-dependent regulation of intracellular G protein signalling is also important to coordinate temporal and spatial order across the SCN. Furthermore, our work extends the role of RGS16 from cellular biology to behaviour. A major challenge in systems neuroscience is to integrate *intra*cellular molecular events with the *inter*cellular neural organization that gives rise to complex behavioural states. Using the SCN as a model, we show that the regulated *intra*cellular G-protein signalling that controls *inter*cellular synchrony across the SCN contributes to the determination of the period of daily rhythms in behaviour.

Methods

Creation of *Rgs16* knockout mice. *Rgs16* mutant mice (Acc. No. CDB0436K: http://www.cdb.riken.jp/arg/mutant%20mice%20list.html) were generated according to our standard method[55]. The targeting vector was constructed using a bacterial artificial chromosome clone containing the mouse *Rgs16* gene (RP24-576N23, BACPAC). We generated the 5′- and 3′-arms of *Rgs16* (Fig. 1d) by PCR and cloned them into the corresponding sites of the DT-A/lox71/LacZ-pA/frt/PGK-Neo/frt/loxP/pA

vector (the details of the vector are available in http://www.cdb.riken.go.jp/arg/cassette.html). Gene targeting was carried out in TT2 cells[56], an embryonic stem cell line established from F1 embryo between C57BL/6J female and CBA male (50% C57BL/6J, 50% CBA). Chimeric males were bred to wild type C57BL/6J females producing F1N0 progeny (75% C57BL/6J, 25% CBA). Germline transmission was verified by PCR as well as Southern blotting on tail DNA. F1N0 males were further backcrossed with C57BL/6J females to create F1N1 progeny (87.5% C57BL/6J). For behavioural analysis (Fig. 1i,j), we continued back-crossing up to F1N10 generation, which corresponds to 12 times backcrossing to the C57BL/6J background (>99.9% C57BL/6J) as the F1N0 mice with which we started back-crossing were already 75% C57BL/6J background. To conduct biochemical and histological analyses, we used F1N5 generation mice (~99.2% C57BL/6J), the behavioural phenotypes of which are equivalent to those of F1N10 mice (free-running period (h) of F1N5 generation mice: *Rgs16*$^{+/+}$, 23.58±0.03 (s.e.m.), *Rgs16*$^{-/-}$, 24.35±0.03, $n=6$ for each genotype, $P<0.01$, *t*-test). We analysed littermate wild-type control mice having equivalent genetic backgrounds than the mutant mice. To this end, males and females from a specific generation (either F1N5 or F1N10 mice) were interbred to create a large colony. No difference in gross morphology or fertility was detected between the genotypes. Unless otherwise mentioned, *in vivo* comparative analyses of WT and mutant mice were conducted in DD. All the studies were approved by the animal experimentation committee of Kyoto University.

Behavioural activity monitoring. Single caged adult *Rgs16*$^{-/-}$ mice and their wild-type littermates (male, 8–15 weeks old) were housed individually in light-tight, ventilated closets within a temperature- and humidity-controlled facility. The animals were entrained on a 12-h-light (~200 lux fluorescent light)–12-h-dark cycle at least two weeks and then transferred to DD. Locomotor activity was detected with passive (pyroelectric) infra-red sensors (FA-05 F5B; Omron)[24,57] and the data obtained were analysed with Clocklab software (Actimetrics) developed on MatLab (Mathworks). Free-running period was determined with either a χ^2 periodogram or a linear regression line fit to the activity onsets. The data used for period measurements were based on animal behaviours in a 14-day interval taken 3 days after the start of DD condition. For the pulse-induced shift experiments, mice put in DD were exposed to a 15 min light pulse at either CT14 or CT22. Phase shifts (delay at CT14, advance at CT22) were quantified as the time difference between regression lines of activity onset before and after the light application.

Microdissection of the mouse SCN. The microdissection of the SCN was performed as described[27] with slight modifications. In brief, animals kept in DD were killed by cervical dislocation, and the eyes were removed under a safety red light. The brain was then isolated from the skull under room light and frozen immediately on dry ice. Coronal brain section (300 μm thick) containing the SCN was prepared using a cryostat microtome (CM3050S, Leica) and mounted on a silicon rubber stage at −17 °C. Under a magnifying glass, the bilateral SCN was punched out from the frozen section using a blunt 20-gauge syringe needle whose edge had been sharpened by filing. For the analysis of circadian expression of RGS16 and Gαi (Fig. 2b), the SCN punches ($n=3$, for each time point) were pooled in Laemmli buffer, and the lysates were subjected to Western blot analysis with antibodies to RGS16 and Gαi. We generated rabbit polyclonal RGS16 antibody. The details of the antibodies used are available in Supplementary Methods.

Pull down assay with His-tagged RGS16. RGS16 binding assay was performed as described[58] with slight modifications. In brief, the SCN punches ($n=5$) were pooled in 300 μl of pull-down buffer (20 mM Na-HEPES, pH 8.0, 380 mM NaCl, 3 mM DTT, 6 mM $MgCl_2$) and homogenized by sonication at 4 °C (Bioruptor, COSMO BIO). The homogenate was divided into two aliquots and incubated with His-RGS16 protein (10 μg) in the presence of either GDP (10 μM) or GDP (10 μM) plus AlF_4^- (30 μM) for 30 min at 4 °C. The reaction mixtures were then treated with 1% cholate and centrifuged at 105,000 *g* (Optima MAX ultracentrifuge, Beckman). The detergent-soluble protein extracts were incubated with Ni2 + -NTA agarose beads (Qiagen) for 15 min at 4 °C. Following three time washes with pull-down buffer supplemented with 20 mM imidazole (plus 10 μM GDP with or without 30 μM AlF_4^-), the beads were boiled in Laemmli buffer. The protein complexes copurified with His-tagged RGS16 were analysed by Western blot.

Immunoprecipitation with RGS16 antibody. Immunoprecipitaion (IP) of RGS16 was performed with the SCN protein extracts from *Rgs16*$^{+/+}$ and *Rgs16*$^{-/-}$ mice. The microdissected SCN punches ($n=5$, for each pool) were homogenized in 300 μl of IP buffer (20 mM Na-HEPES, pH 8.0, 380 mM NaCl, 3 mM DTT, 6 mM $MgCl_2$,10 μM GDP and 30 μM AlF_4^-) by sonication at 4 °C (Bioruptor, COSMO BIO). The homogenates were treated with 1% cholate and then centrifuged at 105,000 *g* (Optima MAX, Beckman). The detergent-soluble protein extracts were subjected to IP with RGS16 antibody and Protein A-Sepharose beads. After three time washes with IP buffer, the beads were boiled in Laemmli buffer. The proteins precipitated with RGS16 antibody were analysed by Western blot.

cAMP measurement. cAMP concentration was determined by enzyme immunoassay (EIA) using cAMP EIA kit (Cayman Chemical) according to the manufacturer's protocol. The microdissected SCN (one punch per assay) was collected in 300 μl of 0.1 N HCl solution and then sonicated at 4 °C (Bioruptor, COSMO BIO). The protein content was determined with BCA Protein Assay kit (Takara). Following centrifugation at 1,000 *g* for 10 min, the supernatant was diluted 1:2 with EIA buffer (Cayman Chemical). All SCN samples underwent acetylation before determination of cAMP level by EIA. We conducted the assays in duplicate, with measurement at l = 405 nm on a plate reader (ARVO, Perkin-Elmer).

***Per1-luc* SCN slice culture**. *Per1-luc* transgenic mice carry a firefly luciferase reporter gene linked to a 7.2 kb genomic DNA fragment covering the 5′ upstream region of the mouse *Per1* gene[59]. *Per1-luc-Rgs16*$^{-/-}$ mice were generated by crossing *Per1-luc* transgenic mice and *Rgs16*$^{-/-}$ mice. The SCN slices were prepared according to our standard method[6] and kept at 35 °C in a sealed 35 mm petri dish with 1 ml of the culture medium containing 1 mM luciferin. The bioluminescence from the cultured SCN was measured with a highly sensitive cryogenic CCD camera (Spectra Video SV16KV/CT: Pixelvision) equipped with a microscope (Axiovert 135TV: Carl Zeiss). Observed data of images were filtered through a median filter to eliminate cosmic-ray-induced background noise. The luminescence was recorded every 20 min. Periods of SCN luminescence recordings were estimated using Fast Fourier Transform—Nonlinear Least Squares analysis[60] as part of the Biological Rhythms Analysis Software System (BRASS). For all SCN to be compared, identical segments of raw SCN luminescence values, starting from the first trough since the start of the measurement, and containing at least four complete cycles, were analysed. BRASS has been developed by Dr Brown PE and co-workers and is available from http://millar.bio.ed.ac.uk/Downloads.html.

Intraventricular infusion of THFA. THFA (Tocris) was continuously delivered to the SCN via osmotic pump as described[29]. In brief, the tip of the infusion cannula (Alzet, Brain Infusion Kit 2) was directed stereotaxically to the SCN and the osmotic pump (Alzet, pump model 1002) containing 100 mM THFA (118 μg/day, infused at 0.24 μl/h) was placed in a subcutaneous pouch by surgery under anaesthesia. We performed the surgery during the subjective daytime (CT8-10) when the phase of circadian clock is considered irresponsive to light. Following the surgery, animals were returned to their home cages and maintained in DD.

Statistical analysis. For the experiments in which three or more test groups were compared, we used one-way analysis of variance (ANOVA) with Bonferroni *post-hoc* test and evaluated the differences derived from genotypes and circadian time points tested. To assess the difference of circadian rhythm (phase) between the zones in *Per1-luc* SCN slices, we analysed the interaction between zone and circadian time with two-way repeated measures ANOVA, followed by Bonferroni's multiple comparison test.

Additional methods. Specific reagents and detailed methodology for DNA microarray analysis, *in situ* hybridization, X-gal staining, immunoblotting, immunohistochemistry and the antibodies used are all described in Supplementary Methods. Microarray data has been deposited in the Gene Expression Omnibus under accession code GSE28574.

References

1. Ralph, M. R., Foster, R. G., Davis, F. C. & Menaker, M. Transplanted suprachiasmatic nucleus determines circadian period. *Science* **247,** 975–978 (1990).
2. Silver, R., LeSauter, J., Tresco, P. A. & Lehman, M. N. A diffusible coupling signal from the transplanted suprachiasmatic nucleus controlling circadian locomotor rhythms. *Nature* **382,** 810–813 (1996).
3. Sujino, M. *et al.* Suprachiasmatic nucleus grafts restore circadian behavioural rhythms of genetically arrhythmic mice. *Curr. Biol.* **13,** 664–668 (2003).
4. Welsh, D. K., Logothetis, D. E., Meister, M. & Reppert, S. M. Individual neurons dissociated from rat suprachiasmatic nucleus express independently phased circadian firing rhythms. *Neuron* **14,** 697–706 (1995).
5. Quintero, J. E., Kuhlman, S. J. & McMahon, D. G. The biological clock nucleus: a multiphasic oscillator network regulated by light. *J. Neurosci.* **23,** 8070–8076 (2003).
6. Yamaguchi, S. *et al.* Synchronization of cellular clocks in the suprachiasmatic nucleus. *Science* **302,** 1408–1412 (2003).
7. Liu, A. C. *et al.* Intercellular coupling confers robustness against mutations in the SCN circadian clock network. *Cell* **129,** 605–616 (2007).
8. Aton, S. J., Colwell, C. S., Harmar, A. J., Waschek, J. & Herzog, E. D. Vasoactive intestinal polypeptide mediates circadian rhythmicity and synchrony in mammalian clock neurons. *Nat. Neurosci.* **8,** 476–483 (2005).
9. Maywood, E. S. *et al.* Synchronization and maintenance of timekeeping in suprachiasmatic circadian clock cells by neuropeptidergic signalling. *Curr. Biol.* **16,** 599–605 (2006).
10. Welsh, D. K., Takahashi, J. S. & Kay, S. A. Suprachiasmatic nucleus: cell autonomy and network properties. *Annu. Rev. Physiol.* **72,** 551–577 (2010).
11. Yan, L. & Okamura, H. Gradients in the circadian expression of Per1 and Per2 genes in the rat suprachiasmatic nucleus. *Eur. J. Neurosci.* **15,** 1153–1162 (2002).

12. Hamada, T., Antle, M. C. & Silver, R. Temporal and spatial expression patterns of canonical clock genes and clock-controlled genes in the suprachiasmatic nucleus. *Eur. J. Neurosci.* **19,** 1741–1748 (2004).
13. Reppert, S. M. & Weaver, D. R. Coordination of circadian timing in mammals. *Nature* **418,** 935–941 (2002).
14. Hastings, M. H., Maywood, E. S. & O'Neill, J. S. Cellular circadian pacemaking and the role of cytosolic rhythms. *Curr. Biol.* **18,** R805–R815 (2008).
15. Liu, A. C., Lewis, W. G. & Kay, S. A. Mammalian circadian signalling networks and therapeutic targets. *Nat. Chem. Biol.* **3,** 630–639 (2007).
16. Yamaguchi, S. *et al.* Role of DBP in the circadian oscillatory mechanism. *Mol. Cell. Biol.* **20,** 4773–4781 (2000).
17. Mitsui, S., Yamaguchi, S., Matsuo, T., Ishida, Y. & Okamura, H. Antagonistic role of E4BP4 and PAR proteins in the circadian oscillatory mechanism. *Genes Dev.* **15,** 995–1006 (2001).
18. Doi, M., Okano, T., Yujnovsky, I., Sassone-Corsi, P. & Fukada, Y. Negative control of circadian clock regulator E4BP4 by casein kinase Iepsilon-mediated phosphorylation. *Curr. Biol.* **14,** 975–980 (2004).
19. Akashi, M., Ichise, T., Mamine, T. & Takumi, T. Molecular mechanism of cell-autonomous circadian gene expression of Period2, a crucial regulator of the mammalian circadian clock. *Mol. Biol. Cell* **17,** 555–565 (2006).
20. Ohno, T., Onishi, Y. & Ishida, N. A novel E4BP4 element drives circadian expression of mPeriod2. *Nucleic Acids Res.* **35,** 648–655 (2007).
21. Ueda, H. R. *et al.* System-level identification of transcriptional circuits underlying mammalian circadian clocks. *Nature Genet.* **37,** 187–192 (2005).
22. Travnickova-Bendova, Z., Cermakian, N., Reppert, S. M. & Sassone-Corsi, P. Bimodal regulation of mPeriod promoters by CREB-dependent signalling and CLOCK/BMAL1 activity. *Proc. Natl Acad. Sci. USA* **99,** 7728–7733 (2002).
23. Balsalobre, A., Marcacci, L. & Schibler, U. Multiple signalling pathways elicit circadian gene expression in cultured Rat-1 fibroblasts. *Curr. Biol.* **10,** 1291–1294 (2000).
24. Shigeyoshi, Y. *et al.* Light-induced resetting of a mammalian circadian clock is associated with rapid induction of the mPer1 transcript. *Cell* **91,** 1043–1053 (1997).
25. Akiyama, M. *et al.* Inhibition of light- or glutamate-induced mPer1 expression represses the phase shifts into the mouse circadian locomotor and suprachiasmatic firing rhythms. *J. Neurosci.* **19,** 1115–1121 (1999).
26. Field, M. D. *et al.* Analysis of clock proteins in mouse SCN demonstrates phylogenetic divergence of the circadian clockwork and resetting mechanisms. *Neuron* **25,** 437–447 (2000).
27. Yamazaki, S., Maruyama, M., Cagampang, F. R. & Inouye, S. T. Circadian fluctuations of cAMP content in the suprachiasmatic nucleus and the anterior hypothalamus of the rat. *Brain Res.* **651,** 329–331 (1994).
28. Obrietan, K., Impey, S., Smith, D., Athos, J. & Storm, D. R. Circadian regulation of cAMP response element-mediated gene expression in the suprachiasmatic nuclei. *J. Biol. Chem.* **274,** 17748–17756 (1999).
29. O'Neill, J. S., Maywood, E. S., Chesham, J. E., Takahashi, J. S. & Hastings, M. H. cAMP-dependent signalling as a core component of the mammalian circadian pacemaker. *Science* **320,** 949–953 (2008).
30. Bansal, G., Druey, K. M. & Xie, Z. R4 RGS proteins: regulation of G-protein signalling and beyond. *Pharmacol. Ther.* **116,** 473–495 (2007).
31. Chen, C., Zheng, B., Han, J. & Lin, S. C. Characterization of a novel mammalian RGS protein that binds to Galpha proteins and inhibits pheromone signalling in yeast. *J. Biol. Chem.* **272,** 8679–8685 (1997).
32. Beadling, C., Druey, K. M., Richter, G., Kehrl, J. H. & Smith, K. A. Regulators of G protein signalling exhibit distinct patterns of gene expression and target G protein specificity in human lymphocytes. *J. Immunol.* **162,** 2677–2682 (1999).
33. Ueda, H. R. *et al.* A transcription factor response element for gene expression during circadian night. *Nature* **418,** 534–539 (2002).
34. Panda, S. *et al.* Coordinated transcription of key pathways in the mouse by the circadian clock. *Cell* **109,** 307–320 (2002).
35. Huang, J. *et al.* Feeding and fasting controls liver expression of a regulator of G protein signalling (Rgs16) in periportal hepatocytes. *Comp. Hepatol.* **5,** 8 (2006).
36. Gerstner, J. R., Vander Heyden, W. M., Lavaute, T. M. & Landry, C. F. Profiles of novel diurnally regulated genes in mouse hypothalamus: expression analysis of the cysteine and histidine-rich domain-containing, zinc-binding protein 1, the fatty acid-binding protein 7 and the GTPase, ras-like family member 11b. *Neuroscience* **139,** 1435–1448 (2006).
37. Aton, S. J., Huettner, J. E., Straume, M. & Herzog, E. D. GABA and Gi/o differentially control circadian rhythms and synchrony in clock neurons. *Proc. Natl Acad. Sci. USA* **103,** 19188–19193 (2006).
38. Okamura, H. Suprachiasmatic nucleus clock time in the mammalian circadian system. *Cold Spring Harb. Symp. Quant. Biol.* **72,** 551–556 (2007).
39. Gachon, F., Olela, F. F., Schaad, O., Descombes, P. & Schibler, U. The circadian PAR-domain basic leucine zipper transcription factors DBP, TEF, and HLF modulate basal and inducible xenobiotic detoxification. *Cell Metab.* **4,** 25–36 (2006).
40. Tominaga, K., Inouye, S. I. & Okamura, H. Organotypic slice culture of the rat suprachiasmatic nucleus: sustenance of cellular architecture and circadian rhythm. *Neuroscience* **59,** 1025–1042 (1994).
41. Sumova, A., Travnickova, Z., Mikkelsen, J. D. & Illnerova, H. Spontaneous rhythm in c-Fos immunoreactivity in the dorsomedial part of the rat suprachiasmatic nucleus. *Brain Res.* **801,** 254–258 (1998).
42. Schwartz, W. J. *et al.* Differential regulation of fos family genes in the ventrolateral and dorsomedial subdivisions of the rat suprachiasmatic nucleus. *Neuroscience* **98,** 535–547 (2000).
43. Obrietan, K., Impey, S. & Storm, D. R. Light and circadian rhythmicity regulate MAP kinase activation in the suprachiasmatic nuclei. *Nature Neurosci.* **1,** 693–700 (1998).
44. Lee, H. S., Nelms, J. L., Nguyen, M., Silver, R. & Lehman, M. N. The eye is necessary for a circadian rhythm in the suprachiasmatic nucleus. *Nature Neurosci.* **6,** 111–112 (2003).
45. Nakaya, M., Sanada, K. & Fukada, Y. Spatial and temporal regulation of mitogen-activated protein kinase phosphorylation in the mouse suprachiasmatic nucleus. *Biochem. Biophys. Res. Commun.* **305,** 494–501 (2003).
46. Graham, T. E., Key, T. A., Kilpatrick, K. & Dorin, R. I. Dexras1/AGS-1, a steroid hormone-induced guanosine triphosphate-binding protein, inhibits 3′,5′-cyclic adenosine monophosphate-stimulated secretion in AtT-20 corticotroph cells. *Endocrinology* **142,** 2631–2640 (2001).
47. Cheng, H. Y. *et al.* Dexras1 potentiates photic and suppresses nonphotic responses of the circadian clock. *Neuron* **43,** 715–728 (2004).
48. von Hayn, K. *et al.* Gq-mediated Ca^{2+} signals inhibit adenylyl cyclases 5/6 in vascular smooth muscle cells. *Am. J. Physiol.* **298,** C324–332.
49. Yoshimura, M. & Cooper, D. M. Cloning and expression of a Ca(2+)-inhibitable adenylyl cyclase from NCB-20 cells. *Proc. Natl Acad. Sci. USA* **89,** 6716–6720 (1992).
50. Chabardes, D., Imbert-Teboul, M. & Elalouf, J. M. Functional properties of Ca^{2+}-inhibitable type 5 and type 6 adenylyl cyclases and role of Ca^{2+} increase in the inhibition of intracellular cAMP content. *Cell. Signal.* **11,** 651–663 (1999).
51. Harmar, A. J. *et al.* The VPAC(2) receptor is essential for circadian function in the mouse suprachiasmatic nuclei. *Cell* **109,** 497–508 (2002).
52. Aton, S. J. & Herzog, E. D. Come together, right.now: synchronization of rhythms in a mammalian circadian clock. *Neuron* **48,** 531–534 (2005).
53. Lema, M. A., Golombek, D. A. & Echave, J. Delay model of the circadian pacemaker. *J. Theor. Biol.* **204,** 565–573 (2000).
54. Locke, J. C., Westermark, P. O., Kramer, A. & Herzel, H. Global parameter search reveals design principles of the mammalian circadian clock. *BMC Syst. Biol.* **2,** 22 (2008).
55. Murata, T. *et al.* ang is a novel gene expressed in early neuroectoderm, but its null mutant exhibits no obvious phenotype. *Gene Expr. Patterns* **5,** 171–178 (2004).
56. Yagi, T. *et al.* A novel ES cell line, TT2, with high germline-differentiating potency. *Anal. Biochem.* **214,** 70–76 (1993).
57. Masubuchi, S., Kataoka, N., Sassone-Corsi, P. & Okamura, H. Mouse Period1 (mPER1) acts as a circadian adaptor to entrain the oscillator to environmental light/dark cycles by regulating mPER2 protein. *J. Neurosci.* **25,** 4719–4724 (2005).
58. Saitoh, O., Kubo, Y., Miyatani, Y., Asano, T. & Nakata, H. RGS8 accelerates G-protein-mediated modulation of K+ currents. *Nature* **390,** 525–529 (1997).
59. Yamaguchi, S. *et al.* The 5′ upstream region of mPer1 gene contains two promoters and is responsible for circadian oscillation. *Curr. Biol.* **10,** 873–876 (2000).
60. Plautz, J. D. *et al.* Quantitative analysis of Drosophila period gene transcription in living animals. *J. Biol. Rhythms* **12,** 204–217 (1997).

Acknowledgments

We thank M. Jounouchi for their expert assistance. This work was supported by Special Coordination Funds for Promoting Science and Technology from the Ministry of Education, Culture, Sports, Science and Technology, the Japanese Government.

Author contributions

M.D. and A.I. are equally contributing first authors. H.O. conceived the project. M.D. and H.O. designed the research. A.I., A.M., M.D. R.T., K.N., S.A. and H.O. created *Rgs16* mutant mice. M.D., A.I., A.M. M.S., R.K., F.Y., I.K., S.T., K.S., Y.Y., M.M., Y.S., H.Y., Y.T., K.O., G.T. and H.O. conducted biochemical and histochemical analyses. M.S., K.S., M.M., J.-M.F. M.K. and H.O. conducted slice culture analyses. H.K., M.A. and M.D. performed mathematical modelling. M.D., K.O., J.-M.F. and H.O. drafted the manuscript.

Additional information

Accession codes: Microarray data has been deposited in the Gene Expression Omnibus under accession code GSE28574.

Supplementary Information accompanies this paper at http://www.nature.com/naturecommunications

Competing financial interests: The authors declare no competing financial interests.

Reprints and permission information is available online at http://npg.nature.com/reprintsandpermissions/

How to cite this article: Doi, M. *et al.* Circadian regulation of intracellular G-protein signalling mediates intercellular synchrony and rhythmicity in the suprachiasmatic nucleus. *Nat. Commun.* 2:327 doi: 10.1038/ncomms1316 (2011).

Supplementary Information for

Circadian regulation of intracellular G-protein signaling mediates intercellular synchrony and rhythmicity in the suprachiasmatic nucleus

Masao Doi[1*], Atsushi Ishida[2*], Akiko Miyake[2], Miho Sato[1], Rie Komatsu[1], Fumiyoshi Yamazaki[1], Ikuo Kimura[3], Soken Tsuchiya[3], Hiroshi Kori[4], Kazuyuki Seo[1], Yoshiaki Yamaguchi[1], Masahiro Matsuo[1], Jean-Michel Fustin[1], Rina Tanaka[1], Yasuko Santo[1], Hiroyuki Yamada[1], Yukari Takahashi[1], Michihiro Araki[5], Kazuki Nakao[6], Shin-ichi Aizawa[6], Masaki Kobayashi[7], Karl Obrietan[8], Gozoh Tsujimoto[3], Hitoshi Okamura[1,2]

To whom correspondence should be addresses: E-mail: okamurah@pharm.kyoto-u.ac.jp

Supplementary Information includes:

Supplementary Figures S1 to S12

Supplementary Methods

Supplementary References

Supplementary Figure S1

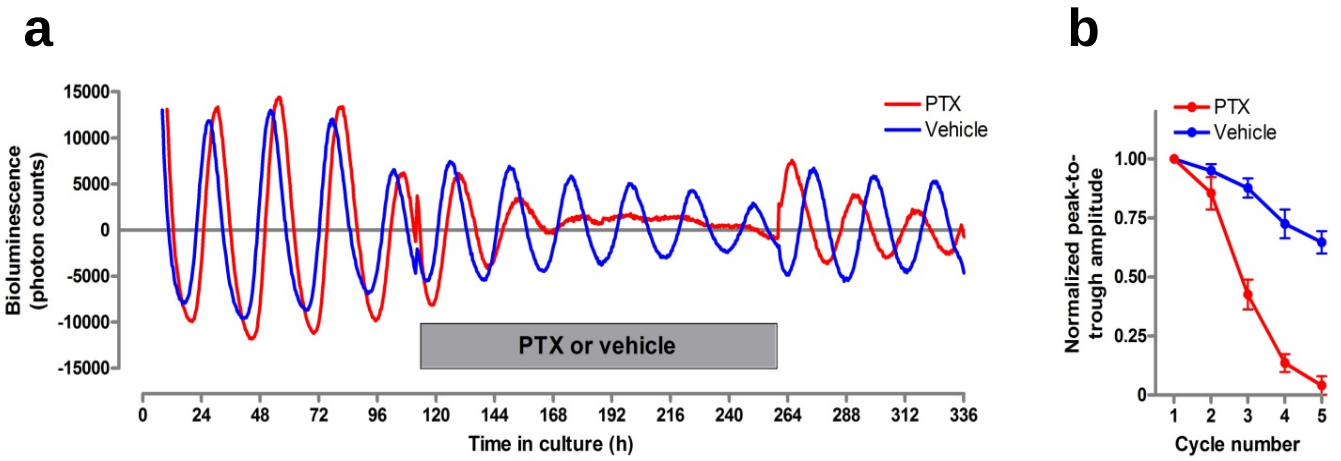

Supplementary Figure S1 | Pertussis toxin dampens *Per1*-luc bioluminescence rhythm in organotypic SCN slice culture. (a) Representative traces of detrended bioluminescence from *Per1-luc* SCN cultures treated with either pertussis toxin (PTX) or vehicle. PTX to a final concentration of five nanomolar was added to the slice culture medium at 112 h, and washed off at 260 h. The bioluminescence from the SCN slice was quantified by a two-dimensional photon-counting camera (Imaging Photon Detector IPD 418, Photek, Essex, UK) linked to a computer workstation continuously recording the data, with an integration time set to 20 minutes (see Methods). Note the progressive loss of consolidated luminescence rhythm from the PTX-treated SCN slice and the recovery of circadian oscillation after PTX washout. **(b)** Mean peak-to-trough amplitudes of rhythms show that PTX-treated slices damped rapidly compared with control slices (n = 3 explants per point, $P < 0.0001$ in two-way ANOVA with Bonferroni post hoc). Data were normalized to the amplitude of the last cycle before drug treatment.

Supplementary Figure S2

a

Gene symbol	RGS subclass	Relative intensity	Affymetrix probe ID	Genbank accession No.
Rgs2	B	598.5	1419248_at	NM_009061
Rgs10	D	443.9	1416882_at	NM_026418
Rgs4	B	297.6	1416286_at	NM_009062
Rgs16	B	212.9	1426037_a_at	NM_011267
Rgs7	C	194.0	1450659_at	NM_011880
Rgs8	B	136.3	1453060_at	NM_026380
Rgs19	A	132.0	1417786_a_at	NM_026446
Rgs20	A	107.3	1443694_at	NM_021374
Rgs3	B	104.7	1425296_a_at	NM_019492
Rgs9	C	78.5	1418691_at	NM_011268
Rgs5	B	73.4	1420941_at	NM_009063
Rgs12	D	47.2	1453129_a_at	NM_173402
Rgs14	D	43.3	1419221_a_at	NM_016758
Rgs11	C	34.1	1425245_a_at	XM_128488
Rgs13	B	5.8	1442263_at	NM_153171
Rgs18	B	5.3	1449856_at	NM_022881
Rgs6	C	3.9	1427340_at	NM_015812
Rgs1	B	3.6	1417601_at	NM_015811
Rgs17	A	N.D.	N.A.	NM_001161822

b

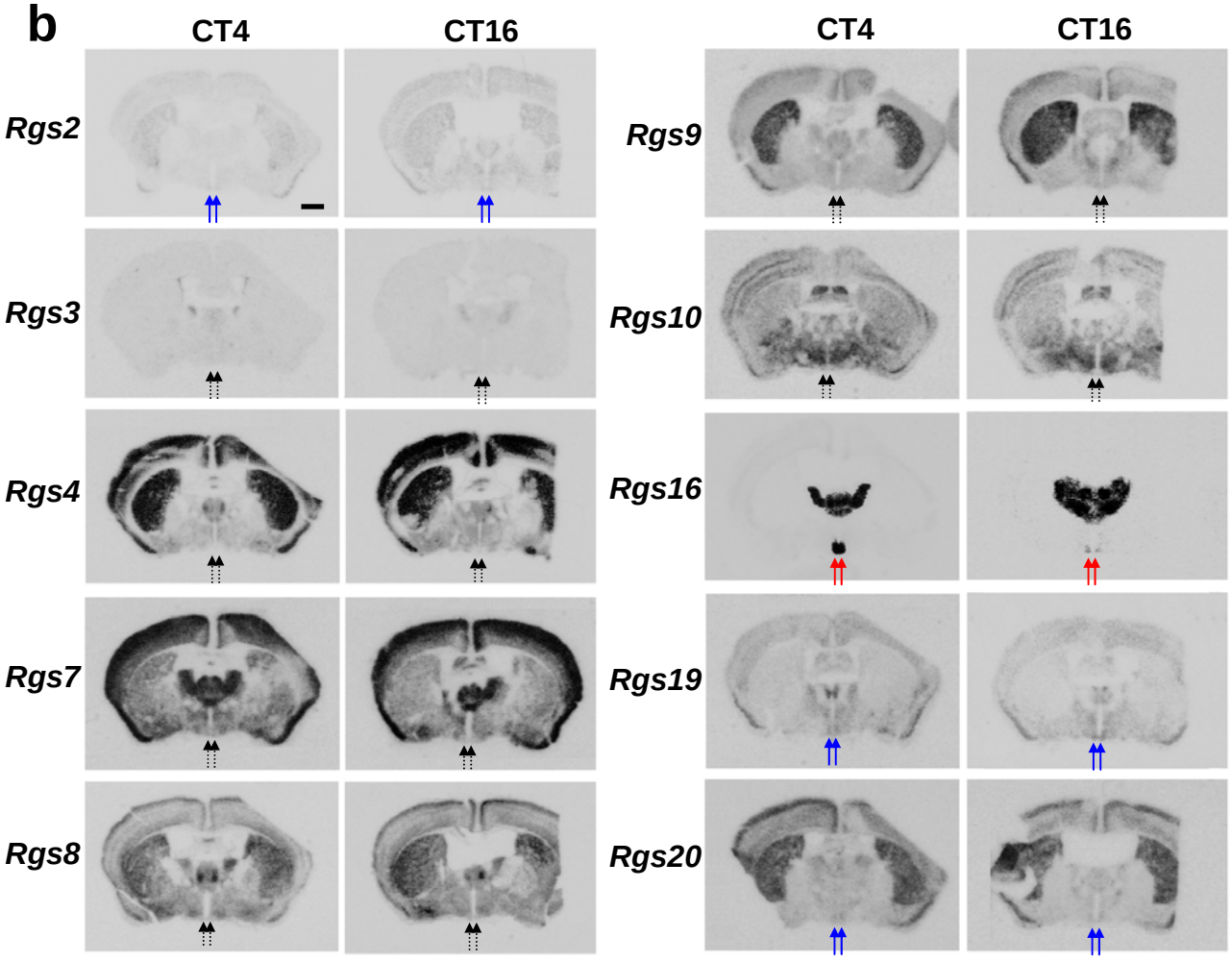

Supplementary Figure S2 | Gene expression profiles of the RGS family in the SCN. (a) SCN microarray analysis focusing on *Rgs* genes that belong to the four major RGS subfamilies (A, B, C, and D), including *Rgs1* to *Rgs20*. From these, 10 most abundant *Rgs* transcripts were selected (*Rgs2*, *Rgs10, Rgs4*, *Rgs16*, *Rgs7*, *Rgs8*, *Rgs19*, *Rgs20*, *Rgs3* and *Rgs9*) and further analyzed with *in situ* hybridization. N.A., not available. N.D. not determined. See Supplementary Methods for details of the microarray analysis. **(b)** Radioisotopic *in situ* hybridization autoradiographs of the genes selected with the mouse coronal brain sections at CT4 and CT16. Note that among the genes selected, *Rgs16* is the only gene whose expression is mainly confined to the SCN with a pronounced day-night variation (red arrows). Solid blue arrows indicate the weakly labeled SCN, and dotted black arrows indicate the negatively stained SCN. Bar, 1 mm

Supplementary Figure S3

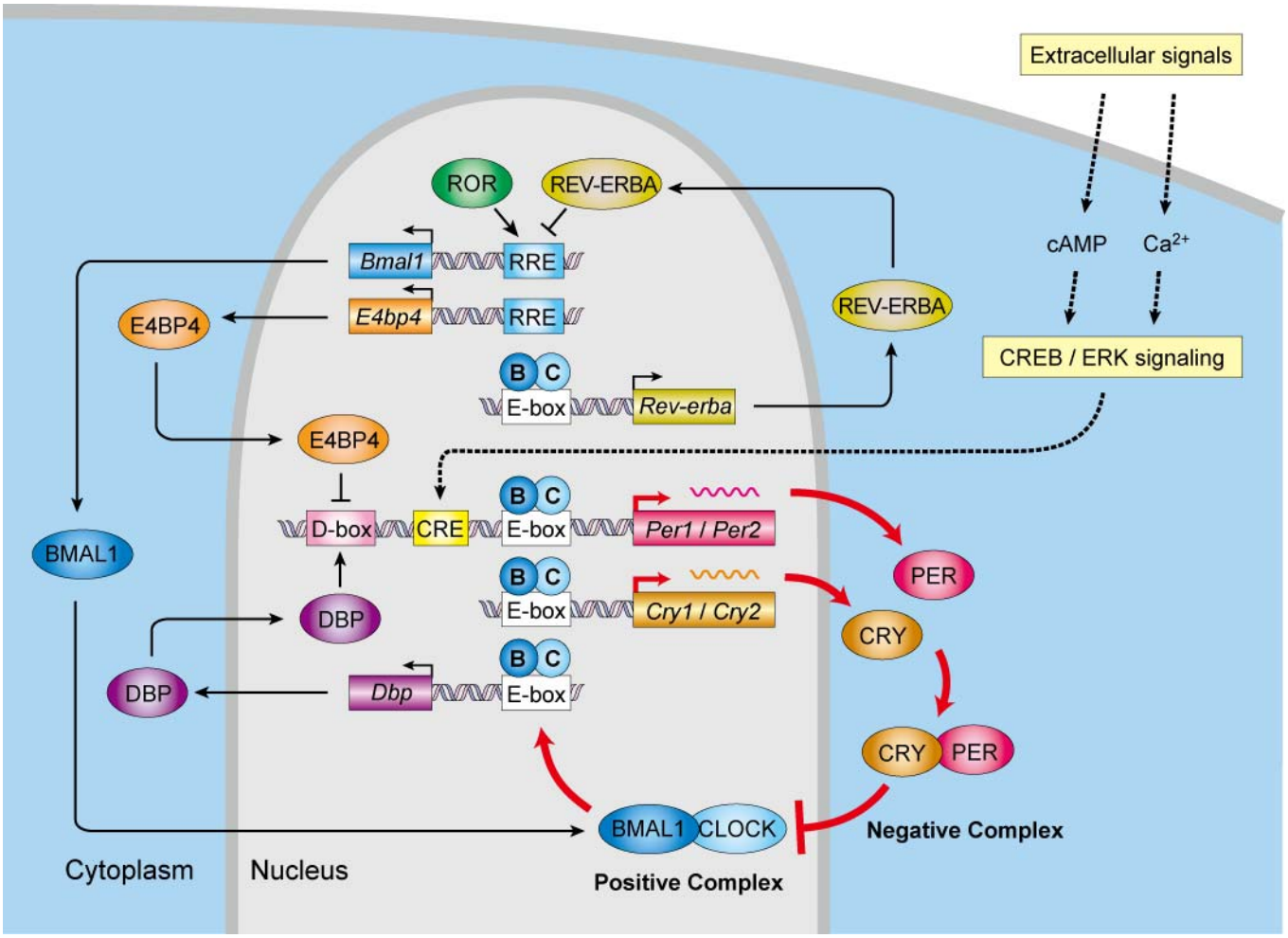

Supplementary Figure S3 | Transcription-translation based feedback loops of the mammalian circadian clock. Heterodimers of CLOCK and BMAL1 activate transcription from the E-box elements, and PER and CRY proteins inhibit the activation. In addition to the autoregulatory feedback loop that regulates cycling at the E-box (termed the ‘‘core loop’’), the PAR bZip family proteins (DBP, TEF and HLF) activate and the related protein E4BP4 represses D-box-mediated transcription, and ROR proteins activate and REV-ERBA proteins repress RRE-mediated transcription, forming interlocking loops. These feedback loops generate the rhythmic expression of not only clock genes, but also of output genes to control the circadian changes in physiology and behavior. Extracellular signals impinge on the intracellular molecular clockwork through activation of CRE-dependent transcription of *Per* genes. This pathway involves Ca^{2+}/cAMP-depdnennt phosphorylation (thus activation) of ERK and CREB.

Supplementary Figure S4

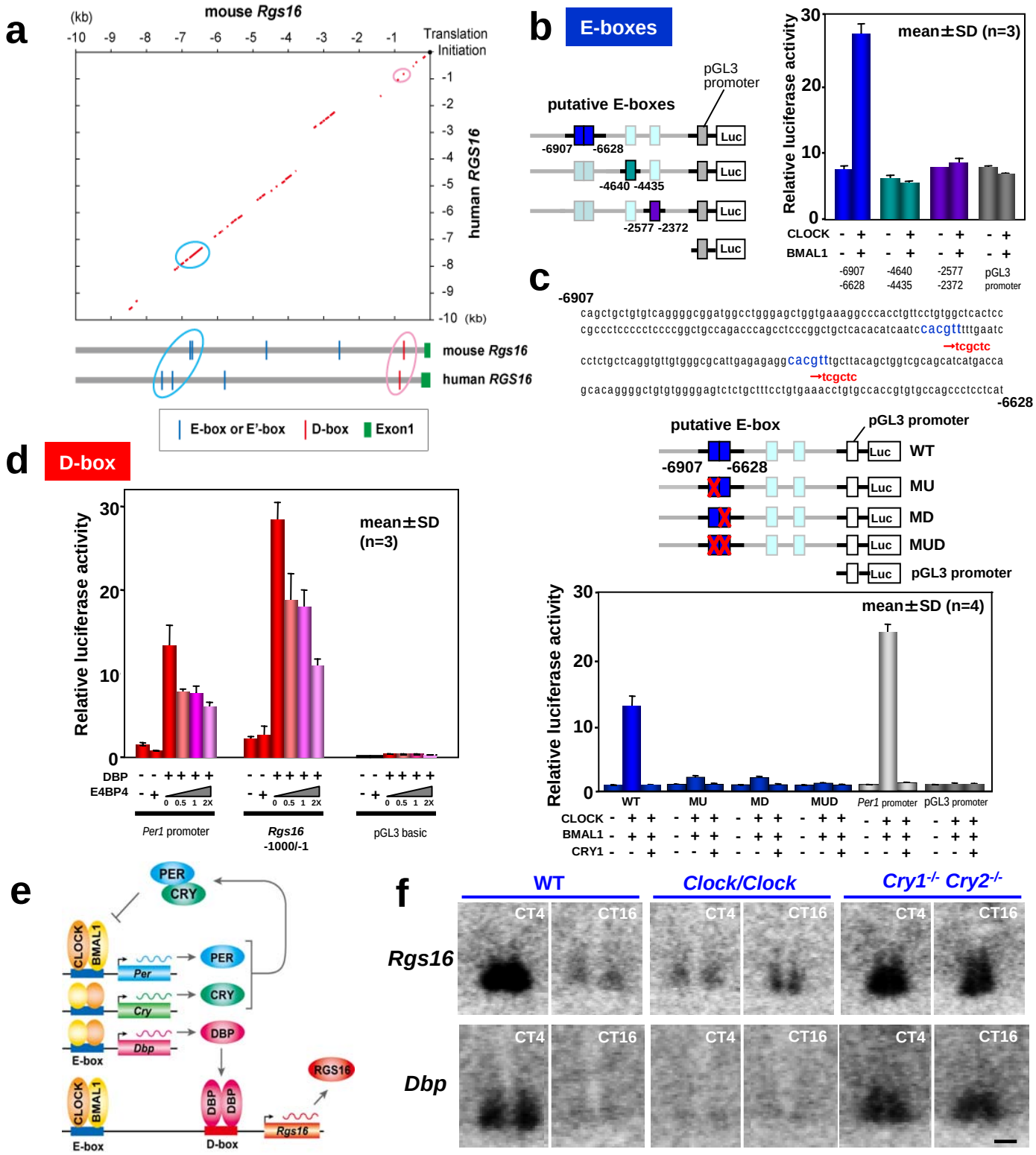

Supplementary Figure S4 | Rgs16 is under transcriptional control of the circadian clock. (a) Dot plot analysis comparing the DNA sequences of human *RGS16* and mouse *Rgs16* 5'-flankling genomic region. Note that the conserved regions contain two serial E-boxes (blue circle) and one D-box (pink circle). **(b-d)** Promoter assay of the mouse *Rgs16* gene. Shown are relative luciferase activities (mean±SD) in cultured NIH3T3 cells after transfection of the indicated luciferase reporters. +, transfection of expression plasmid with insert encoding the indicated protein. **(b,c)** Two serial E-boxes lined side by side in the -6907 to -6628 fragment allows CLOCK and BMAL1 to activate transcription. Mutation of these two E-boxes impairs CLOCK-BMAL1-dependent transactivation. By contrast, the putative E-boxes located in the fragments of -2577 to -2372 and -4640 to -4435 are irresponsive to CLOCK and BMAL1. **(d)** DBP activates transcription through the mouse *Rgs16* promoter containing D-box. E4BP4 antagonizes the DBP-mediated transcription in a dose-dependent manner. As a control for **c** and **d**, we used *Per1* promoter luciferase reporter, which contains functional E-box and D-box (Supplementary Figure S3). **(e)** Model depicting the transcriptional control of *Rgs16* by core clock machinery. CLOCK-BMAL1 complex activates transcription of *Rgs16*, acting not only through E-box but also indirectly through D-box by enhancing the expression of DBP (*Dbp* is an E-box-regulated gene). PER-CRY complex inhibits CLOCK-BMAL1 mediated transcription and reduces DBP expression, both of which lead to the suppression of *Rgs16*. **(f)** Radioisotopic *in situ* hybridization autoradiographs showing the expression of *Rgs16* and *Dbp* in the SCN of WT, *Clock/Clock* and *Cry1*$^{-/-}$*Cry2*$^{-/-}$ mice at CT4 and CT16. Consistent with our model in **e**, the levels of *Rgs16* mRNA in the SCN is constitutively low in *Clock/Clock* mice (upper panels), where the mutation of CLOCK reduces the E-box-dependent transcription and lowers the expression of *Dbp* as well (lower panels). Conversely, the levels of *Rgs16* mRNA is constitutively high in *Cry1*$^{-/-}$*Cry2*$^{-/-}$ mice (upper panels), where the E-box-mediated transcription is kept upregulated. The expression of *Dbp* is also constantly high in these animals (lower panels). Bar, 100 μm

Supplementary Figure S5

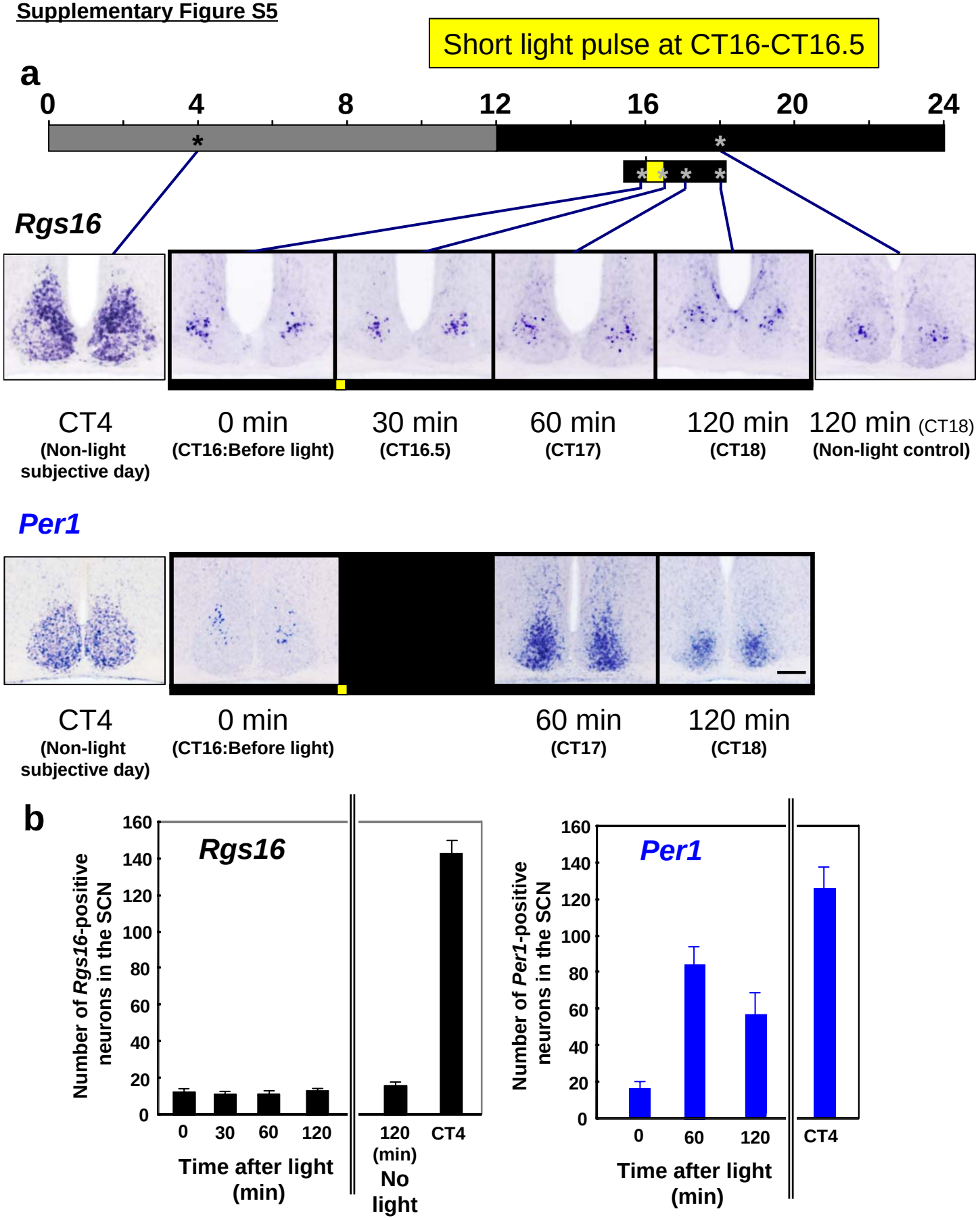

Supplementary Figure S5 | Light pulse does not induce *Rgs16* mRNA expression in the SCN. (a) Representative photomicrographs of digoxigenin *in situ* hybridization for *Rgs16* and *Per1* in the SCN under the indicated light conditions. Mice were exposed to a brief light (200 lux fluorescent light) at CT16 for 30 min and sacrificed 30, 60 and 120 min after the start of the light exposure. No-light-exposed animals at 120 min served as a control group. We also analyzed the expression at CT4 as a reference. Bar, 100 μm. **(b)** Number of positively stained neurons (mean ± s.e.m, $n = 4$ for each experimental group). Note that light does not enhance the expression of *Rgs16* in the SCN, which sharply contrasts with the light-dependent acute induction of *Per1* in the SCN.

Supplementary Figure S6

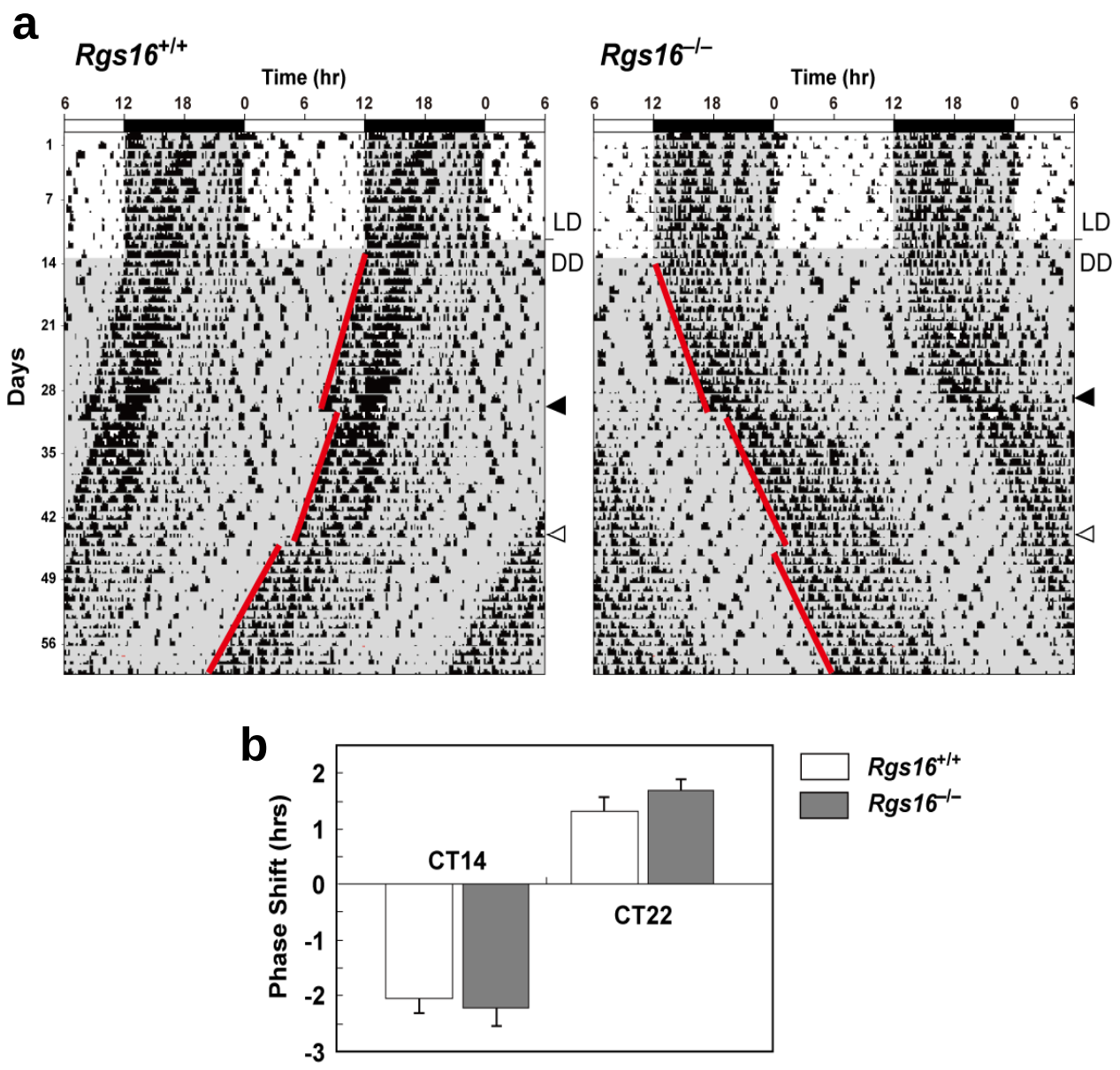

Supplementary Figure S6 | A light pulse causes a phase shift of locomotor activity rhythms of *Rgs16*$^{-/-}$ mice. (a) Representative double-plotted locomotor activity records of *Rgs16*$^{+/+}$ and *Rgs16*$^{-/-}$ mice. Mice were initially housed in a 12L:12D light-dark cycle (LD) and then transferred to constant darkness (DD). A brief light pulse (200 lux fluorescent light, for 15 min) was given at CT14 (on the day indicated by solid arrowheads) and CT22 (open arrowheads), which causes a phase delay and advance, respectively, on the following days. Red lines delineate the phase of activity onset. **(b)** Quantification of the magnitude of phase shifts (n = 10 for each genotype). By convention, delays are negative and advances are positive. Note that WT and mutant mice are virtually the same in the extent of the phase shifts.

Supplementary Figure S7

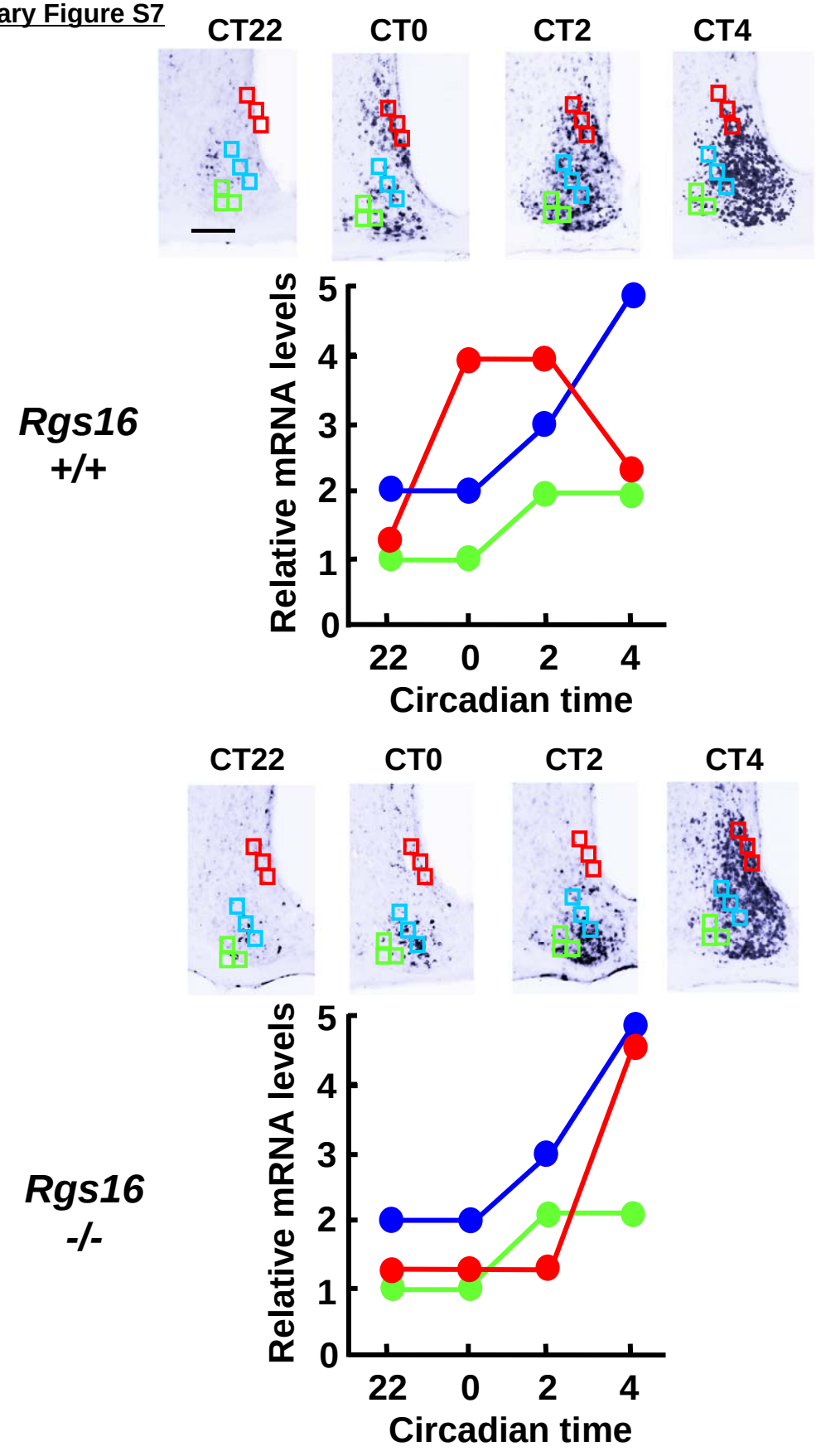

Supplementary Figure S7 | Semi-quantification of temporal changes in *Per1* mRNAs within *in vivo* SCN. *Rgs16*$^{+/+}$ and *Rgs16*$^{-/-}$ mice housed in constant darkness were examined with *in situ* hybridization using the digoxigenin-labeled *Per1* probe. The intensity range of positive signals in an area within dorsal (red), central (blue), and ventral (green) portions is: +5, strongest; +4, very strong; +3, strong; +2, moderate; +1, low; 0, very low to none. CT, circadian time. oc, optic chiasm; v, third ventricle. Bar, 100 μm. WT data are compatible with those of previous reports showing the dorsomedial-ventrolateral gradients of *Per1* expression in the SCN (see refs. 6,11,12 in the main texts).

Supplementary Figure S8

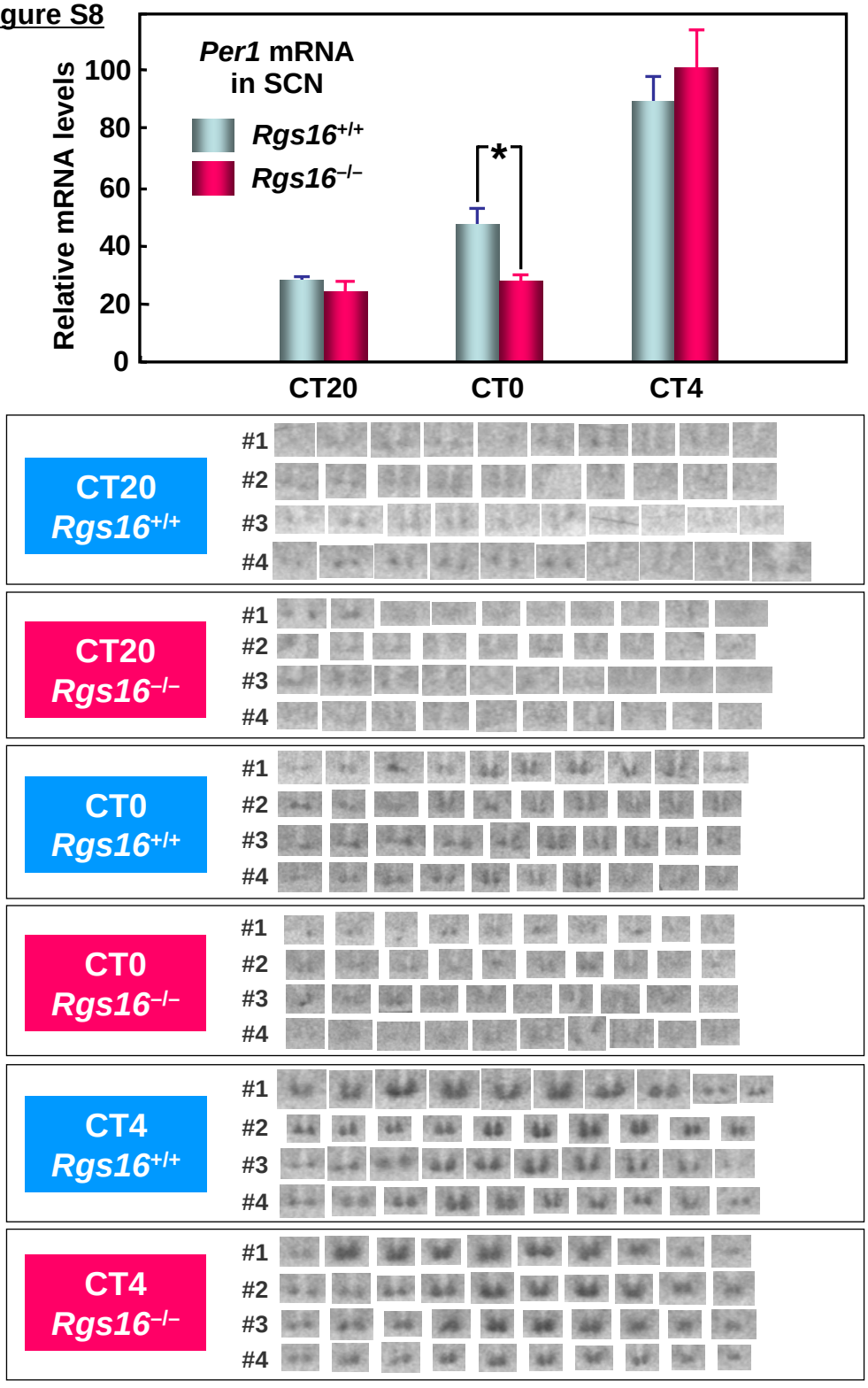

Supplementary Figure S8 | Quantification of temporal changes of *Per1* mRNA signals in the SCN by radioisotopic *in situ* hybridization. *Rgs16*$^{+/+}$ and *Rgs16*$^{-/-}$ mice housed in constant darkness were examined with *in situ* hybridization using the isotope-labeled *Per1* probe. To quantitatively determine the levels of *Per1* mRNA expressed in the whole SCN, serial coronal brain sections (40μm thick), covering from the rostralmost to the caudalmost of the SCN (10 sections per animal), were analyzed. To minimize technical variations throughout the hybridization procedure, all sections from different experimental conditions were gathered into one group and processed simultaneously. To detect isotope signals, we used X-ray film (BioMax, Kodak), and the signal intensity of each SCN on the film was measured using a microcomputer interfaced to an image analyzing system (MCID, Imaging Research Inc., Canada) after conversion into the relative optical densities produced by the 14C-acrylic standards (GE healthcare). Data were normalized with respect to the difference between signal intensities in equal areas of the SCN and the corpus callosum. Then, the intensities of the optical density of the sections from the rostral end to the caudal end of the SCN (10 sections per animal) were summed; the sum was considered a measure of the amount of *Per1* mRNA in this region. Shown are the relative *Per1* mRNA levels (means ± s.e.m.) in *Rgs16*$^{+/+}$ and *Rgs16*$^{-/-}$ mice at the indicated time points (n = 4; animals #1, #2, #3, and #4 for each group), with the average of *Rgs16*$^{-/-}$ at CT4 set to 100. The autoradiographs show the SCN sections used for quantification. For statistical analysis, one-way ANOVA followed by Sheffe's multiple comparisons were applied. *$P < 0.01$.

Supplementary Figure S9

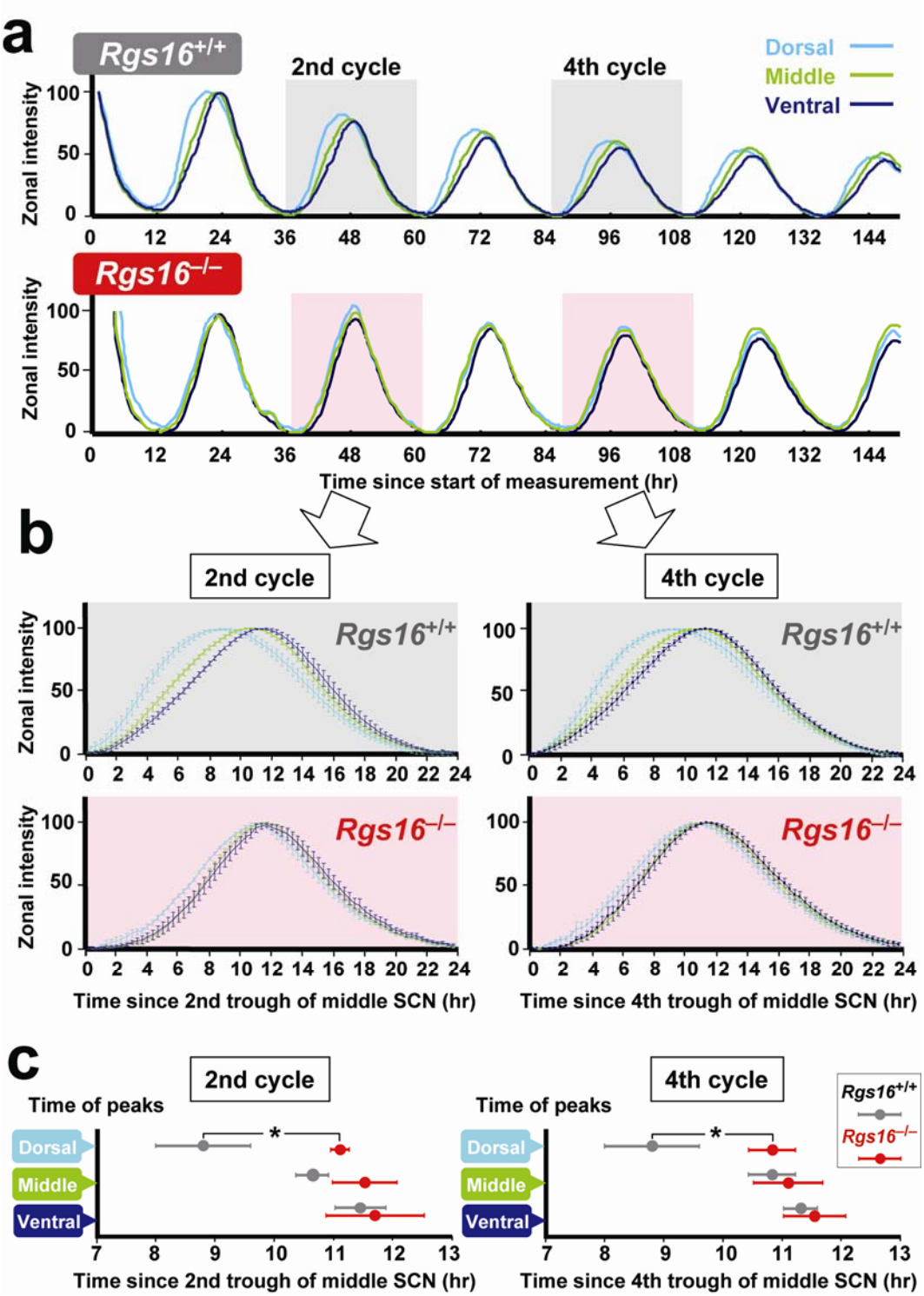

Supplementary Figure S9 | Zonal phase-relationships within *Rgs16*$^{+/+}$ and *Rgs16*$^{-/-}$ SCN slices do not change during the course of culturing. (a) Representative records of zonal luminescence in cultured SCN slices from *Per1-luc*-bearing *Rgs16*$^{+/+}$ and *Rgs16*$^{-/-}$ mice. For non-biased selection of ROI, the SCN was divided into three regions (dorsal, middle, and ventral) with equal proportions along vertical axis (see Fig. 3c). The *x* axis represents time since start of measurement. The intensity of each zone is plotted relative to the first peak value. **(b)** 24 hour temporal profiles of zonal luminescence in *Rgs16*$^{+/+}$ and *Rgs16*$^{-/-}$ slices from either the 2nd (left) or the 4th (right) trough of middle SCN [means ± s.e.m (*n* = 4); the peak and trough values were adjusted to 100 and 0, respectively]. **(c)** The average of peak time (± s.d.) in each zone of *Rgs16*$^{+/+}$ and *Rgs16*$^{-/-}$ slices since the 2nd (left) or 4th (right) trough of middle SCN (n = 4, for each genotype). Two-way analysis of variance with Bonferroni's *post hoc* tests reveal statistically significant difference between WT and *Rgs16*$^{-/-}$ slices only in dorsal zone, but not in middle and ventral zones. **P* < 0.001.

Supplementary Figure S10

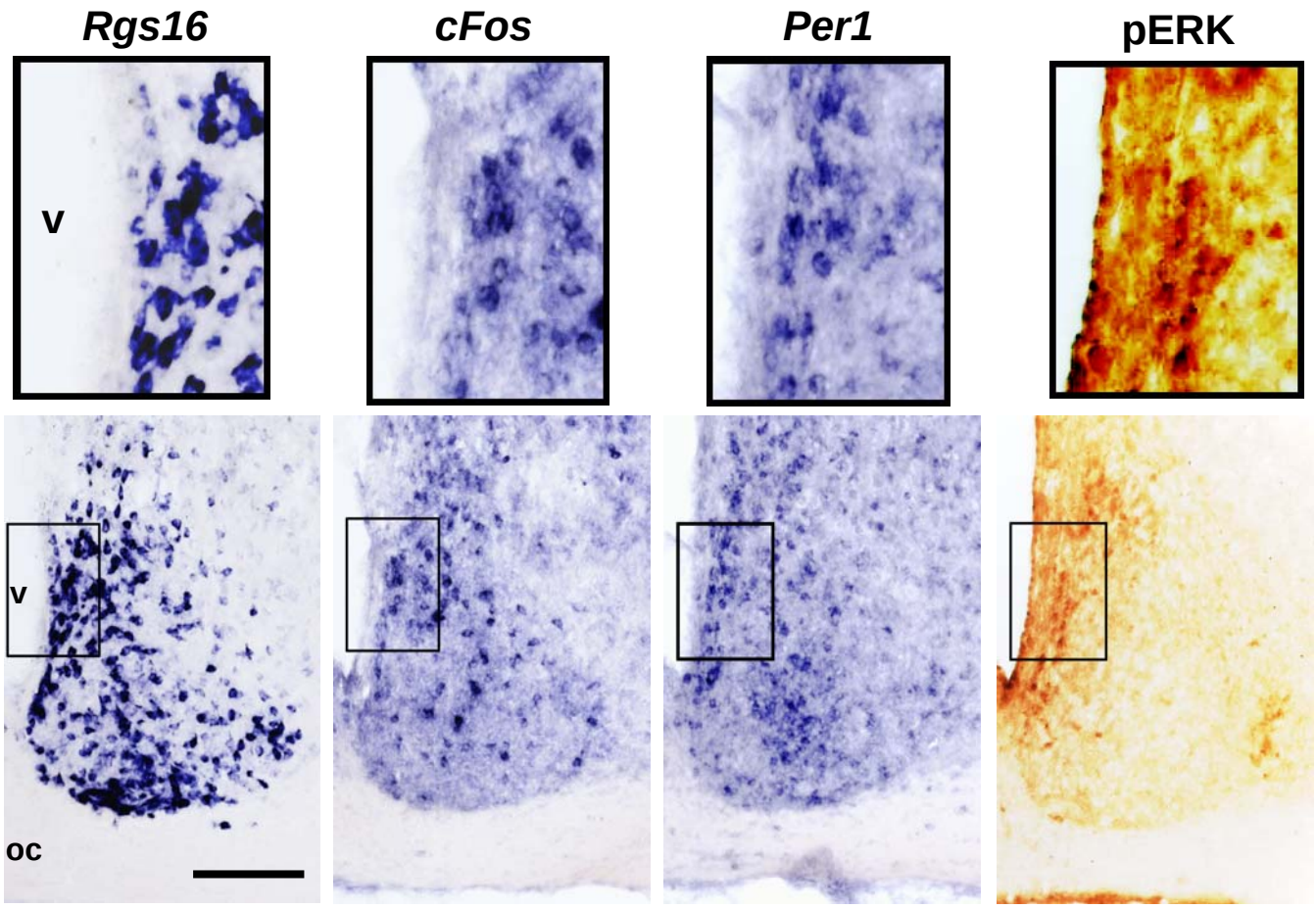

Supplementary Figure S10 | Increased expression of *Rgs16*, *cFos*, *Per1* and pERK at dawn in the periventricular part of the dorsomedial SCN. Representative photomicrographs showing digoxigenin *in situ* hybridization of *Rgs16*, *cFos* and *Per1* and immunohistochemical staining of pERK on serial SCN sections (30 μm in thick) at CT0. Upper panels are higher magnification images of the regions boxed below. oc, optic chiasm; v, third ventricle. Bar, 100 μm.

Supplementary Figure S11

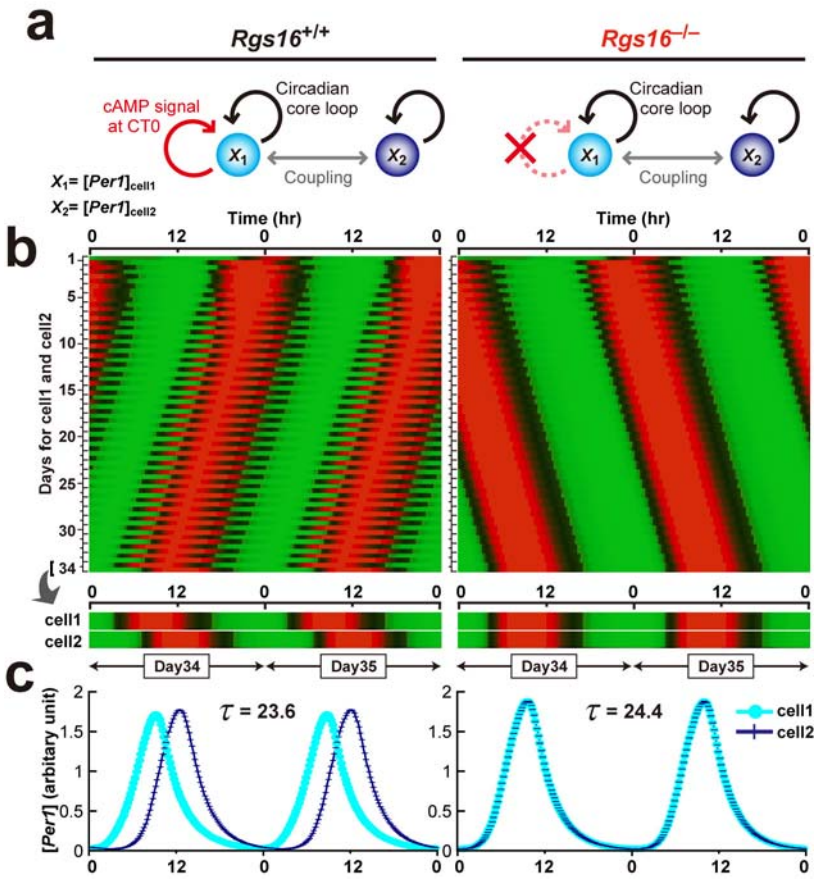

Supplementary Figure S11 | Mathematical simulation of the loss of cAMP-dependent acceleration of *Per1* in the phase-leading cell. (a) Schematic representation of two reciprocally coupled cellular oscillators, cell1 and cell2. These cells are identical except that cell1 has cAMP-dependent enhancement of *Per1* expression at dawn (left). Thus, the deletion of cAMP pathway from cell1 results in the construction of two equivalent oscillators that are mutually coupled in a symmetric fashion (right). **(b)** Raster plots of *Per1* concentrations in cell1 and cell2 for 35 days. For comparison, daily profiles of cell1 and cell2 are aligned each day and presented in a double-plotted format. Values above and below the mean are shown in red and green, respectively. **(c)** Concentrations of *Per1* in cell1 and cell2 on days 34 and 35, representing intercellular phase-relationship of cell1 and cell2 and circadian period (τ, peak-to-peak interval) of their synchronous rhythms.

Supplementary Figure S12

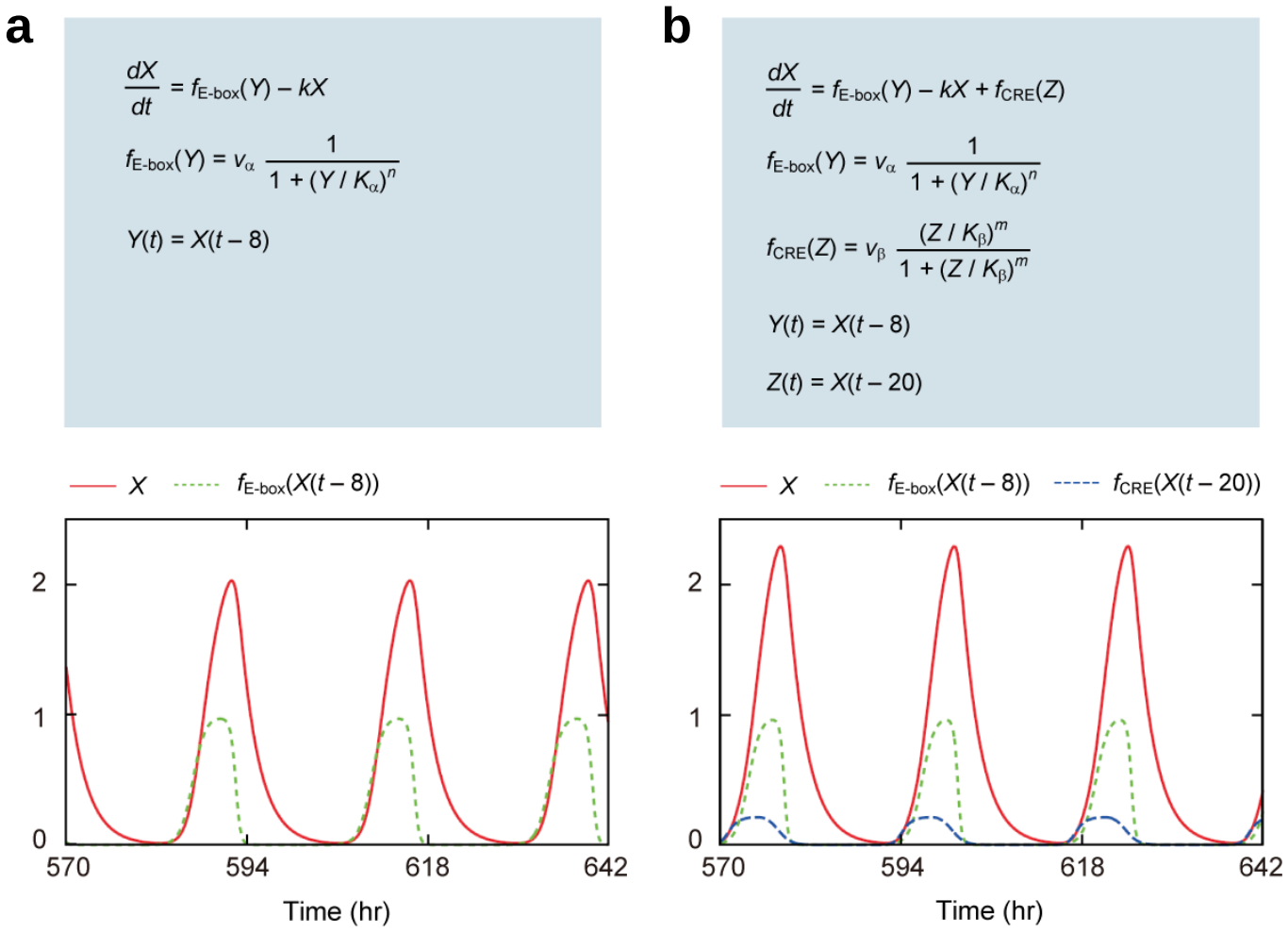

Supplementary Figure S12 | Mathematical simulation for a single-cell oscillator where the term accounting for cAMP signaling at dawn is absent (a) and present (b). Shown are the equations used (upper) and the time course of *X* (red line) during the indicated period (lower). For comparison, the values of $f_{E\text{-box}}(X(t - 8))$ and $f_{CRE}(X(t - 20))$ are also plotted in the lower panels. Numerical setup is as follows. In **a**, $\delta_\alpha = 8.0$, $v_\alpha = 1.0$, $K_\alpha = 0.04$, $n = 3.0$, and $k = 0.4$. In **b**, in addition to the values used in **a**, $v_\beta = 0.23$, $K_\beta = 1.0$, $m = 3.0$. The initial condition was $X(t) \equiv 0.1$ ($-30 < t < 0$). See Supplementary Methods for more details.

Supplementary Methods

In situ hybridization.

In situ hybridization analysis was performed as described[24] with the following gene-specific probes: for *Rgs16*, the anti-sense probe covering nucleotides 24-761 of the *Rgs16* mRNA (GenBank, NM_011267); for *Gnai1*, nucleotides 2401-2998 (NM_010305); for *Gnai2*, nucleotides 1498-2060 (NM_008138); for *Per1*, nucleotides 812-1651 (NM_011065); for *cFos*, nucleotides 1152-1735 (NM_010234); for *Dbp*, nucleotides 15-520 (NM_016974); for *LacZ*, nucleotides 1126-1952 (V00296). for *Rgs2*, nucleotides 1511-2057 (NM_009061); for *Rgs3*, nucleotides 1121-1698 (NM_019492); for *Rgs4*, nucleotides 1519-2003 (NM_009062); for *Rgs7*, nucleotides 982-1643 (NM_011880); for *Rgs8*, nucleotides 4791-5319 (NM_026380); for *Rgs9*, nucleotides 910-1561 (NM_011268); for *Rgs10*, nucleotides 444-846 (NM_026418); for *Rgs19*, nucleotides 725-1215 (NM_026446); for *Rgs20*, nucleotides 778-1327 (NM_001177795).

X-gal staining.

For X-gal labeling of brain sections, *Rgs16*$^{+/-}$ mice were anesthetized and circulationally perfused with 25 ml of cold fixative [2.5% glutaraldehyde in 0.1 M phosphate buffer (PB), pH 7.4]. The isolated brain was post-fixed in the same fixative for 3 hr at 4°C and then transferred to 20% sucrose in 0.1 M PB for cryoprotection. Coronal brain cryosections (30 μm thick) were stained with X-gal for β-galactosidase activity, according to Mombaerts *et al*[62].In brief, the free-float sections were washed twice (5 min and 30 min, respectively) in buffer A (0.1 M PB, 2 mM MgCl2, and 5 mM EGTA); followed by two washes of 5 min at room temperature with buffer B (0.1 M PB, 2 mM MgCl2, 0.01% sodium desoxycholate, and 0.02% Nonidet P40). The sections was then incubated in X-gal staining buffer [buffer B plus 5 mM K-ferricyanide, 5 mM K-ferrocyanide, and X-gal (1 mg/ml)] for 3 hours at room temperature in light-proof containers. The stained sections were coverslipped with mounting medium (Entellan, Merk Chemicals) after dehydration.

Microarray analysis.

Microarray analysis was performed as described[61]. In order to identify genes that are enriched

in the SCN, SCN punches taken from 10 animals at CT2 and 10 animals at CT14 were pooled together into Trizol reagent (Invitrogen). Total RNA was isolated from the lysate using the RNeasy micro kit (Qiagen) and the integrity was assessed by analyzing aliquots on an Agilent 2100 Bioanalyzer (Agilent Technologies). cDNA synthesis and cRNA labelling were performed using the One-Cycle Target Labelling and Control Reagents Kit (Affymetrix), and subsequent hybridization was performed with GeneChip Mouse Genome 430 2.0 array (Affymetrix) according to the manufacture' protocol. The data were normalized with the MAS5 (GCOS 1.4) algorithm, using the default analysis settings and global scaling as normalization method. The resulting value of mean target intensity (TGT) was 111.55.

Generation of RGS16 recombinant protein and antibodies used for Western blot.

The full-length coding sequence of the mouse *Rgs16* (NM_011267) was cloned into either pET45b(+) (Takara) or pGEX6P (GE healthcare) and introduced into *Escherichia coli* strain BL21(DE3). His-tagged RGS16 and GST-fused RGS16 proteins were affinity-purified with Ni2+-NTA agarose (Qiagen) and Glutathione-Sepharose 4B (GE healthcare), respectively. We generated polyclonal antibody to RGS16 by immunizing rabbit with His-tagged RGS16. Then, the raised antibodies were purified using GST-fused RGS16 protein-conjugated column (HiTrap NHS-activated HP, GE healthcare). The Gαi antibody used was purchased from Abcam (G Protein alpha Inhibitor 1+2 antibody, rabbit polyclonal, ab3522). This antibody recognizes both Gαi1 and Gαi2. Western blot was performed according to our standard method[18]. The imunoreactivities were visualized with enhanced chemiluminescence (ECL plus, GE healthcare).

Immunohistochemistry for pERK.

For immunohistochemistry of pERK, animals were anesthetized and circulationally perfused with 25 ml of cold fixative (4% paraformaldehyde in 0.1 M PB). The isolated brains were post-fixed with the same fixative for 12 hr at 4°C and then transferred to 20% sucrose in 0.1M PB for cryoprotection. Coronal brain cryosections (30 μm thick) were processed for free-floating immunohistochemistry with rabbit polyclonal antibody specific for the phosphorylated forms of ERK 1 and 2 (Cell Signaling, #9101): In brief, the free-floating sections, pretreated with hydrogen peroxide (1.5%, in 0.1 M PB, for 20 min at 4°C), were blocked with 5% horse

serum in 0.1 M PB for 1 hr at room temperature. Then, the sections were incubated with the primary antibody [1:500 dilution, in 0.1 M PB containing 0.3% Triton X-100 (PBX)] for 3 days at 4°C. After washing with PBX, the sections were incubated with a secondary antibody [biotinylated anti-rabbit IgG (Vector Laboratories), 1:1000 dilution in PBX] for 12 hr at 4°C. The imunoreactivities were visualized according to a standard avidin-biotin-immunoperoxidase procedure (Vectorstain Elite ABC kit, Vector Laboratories). The immunostained sections were washed with 50 mM Tris-HCl buffer (pH 7.5) and coverslipped with Entellan after dehydration.

Simulation of single-cell oscillator

Our mathematical model is based on a previously published circadian clock model[52,53]. Before explaining the two-coupled oscillator model we used in Supplementary Figure S11, we first briefly review the model describing a single-cell oscillator.

The time-evolution of *Per1* mRNA level (referred to as X) is described as follows:

$$\frac{dX}{dt} = f_{\text{E-box}}(Y) - kX,$$
$$f_{\text{E-box}}(Y) = v_\alpha \frac{1}{1+\left(Y / K_\alpha\right)^n}, \qquad \text{[S1]}$$

where $f_{\text{E-box}}(Y)$ is the *Per1* transcription rate (via circadian core loop); $Y(t)$ is the concentration of repressor (e.g. PER-CRY complex, Supplementary Figure S3); v_α is the maximum *Per1* transcription rate; K_α is the dissociation constant; n is the Hill coefficient; k is the degradation constant. We define the time unit as hours, while the units of other quantities are left to be arbitrary. Lema *et al.*[52] assumed that $Y(t)$ evolves in the same manner as $X(t)$ but with a time lag (δ_α).

$$Y(t) = X(t - \delta_\alpha) \qquad \text{[S2]}$$

This equation makes it possible to describe the self-sustained circadian oscillation just using one variable[52]. By choosing appropriate parameter values, a robust oscillation of X can be obtained. The graph shown in Supplementary Figure S12a displays a time-series of $X(t)$ and $f_{\text{E-box}}(X(t - \delta_\alpha))$ numerically obtained from equation [S1] for $\delta_\alpha = 8.0$, $v_\alpha = 1.0$, $K_\alpha = 0.04$, $n = 3.0$, and $k = 0.4$.

We then added the term accounting for the cAMP signaling at dawn to the model [S1] as follows:

$$\frac{dX}{dt} = f_{\text{E-box}}(Y) - kX + f_{\text{CRE}}(Z),$$
$$f_{\text{CRE}}(Z) = v_\beta \frac{\left(Z / K_\beta\right)^m}{1 + \left(Z / K_\beta\right)^m}, \qquad \text{[S3]}$$

where $f_{\text{CRE}}(Z)$ is the *Per1* transcription rate by cAMP signaling, Z is the concentration of the CRE activator (e.g., pCREB, Supplementary Figure S3), v_β is the maximum *Per1* transcription rate, K_β is the dissociation constant, and m is the Hill coefficient. Similar to the equation [S2] for $Y(t)$, we express $Z(t)$ as follows:

$$Z(t) = X(t - \delta_\beta) \qquad \text{[S4]}$$

Here, δ_β represents a time lag between Z and X. Our experimental data indicate that the expression of *cFos* in the dorsomedial phase-leading cells reaches the peak at CT0, which precedes the peak of the *Per1* expression in the ventral SCN at CT4. We thus postulate that the peak of the cAMP signaling (reflected by *cFos*) is 4 h advanced (or 20 h delayed) relative to that of the activation of E-box-dependent transcription (reflected by *Per1* in the *cFos*-negative cells). Since our simulations do not use negative delay, we set the value of δ_β to 20 h, instead of – 4 h (so that the value of Z can be extrapolated from a reference point of X in the past time). The graph shown in Supplementary Figure S12b displays $X(t)$, $f_{\text{E-box}}(Y)$, and $f_{\text{CRE}}(Z)$ numerically obtained from equation [S3] for $\delta_\beta = 20$, $v_\beta = 0.23$, $K_\beta = 1.0$, $m = 3.0$ (and other parameters are the same as those in Supplementary Figure S12a). Note that in this model, $f_{\text{CRE}}(Z)$ begins to increase earlier than $f_{\text{E-box}}(Y)$.

Simulation of two coupled oscillators

We extended our analysis to two coupled oscillators, cell1 and cell2 (Supplementary Figure S11). Because the autonomous expression of *cFos* at dawn is a feature specific to phase-leading cell, we added the term for cAMP signaling [i.e. $f_{\text{CRE}}(Z)$] to only one of the two cells. This reflects the heterogeneity of cells in the SCN. Although it can not be excluded that in a certain SCN neurons, alternative cAMP pathway may operate without simultaneous *cFos* expression,

we omitted this unknown cAMP pathway from our settings for the sake of concision. We focused on the simulations with or without cAMP signaling at dawn within one of the two cells. We constructed a model in which cell1 (with cAMP) and cell2 (without cAMP) are mutually coupled as follows:

$$\begin{aligned}\frac{dX_1}{dt} &= f_{\text{E-box}}(Y_1) - kX_1 + v_\gamma \frac{F}{1+F} + f_{\text{CRE}}(Z_1), \\ \frac{dX_2}{dt} &= f_{\text{E-box}}(Y_2) - kX_2 + v_\gamma \frac{F}{1+F},\end{aligned} \qquad \text{[S5]}$$

where X_i and Y_i, are the concentrations of the *Per1* mRNA and the repressor in cell i (i = 1, 2), respectively. The term corresponding to the cAMP signaling at dawn appears only for cell1. The third terms on the right hand sides describe the *Per1* transcription rates via intercellular coupling. F is a coupling mediator and expressed as $F(t) = X_1(t) + X_2(t)$, and v_γ is the maximum *Per1* transcription rate via intercellular coupling. This coupling form is similar to that proposed by Loche *et al.*[53]. Although the biological plausibility of this coupling form is unclear, we expect that the results shown in Supplementary Figure S11 do not strongly depend on the mode of the coupling form tested, if the coupling tends to make the oscillators synchronized. Actually, we had tested a different coupling form, proposed by Liu *et al.*[7], and we found that the results obtained were essentially the same as those in Supplementary Figure S11 (data not shown).

As shown in Supplementary Figure S11, we performed numerical simulations using the model [S5] with equations [S2] and [S4]. The parameter values used were the same as those for Supplementary Figure S12. $v_\gamma = 0.07$. The initial conditions were set as follows: $X_1(t) = 0.1$, $X_2(t) = 1.0$ $(-30 \le t \le 0)$. Intriguingly, under the condition that $v_\beta = 0.23$ (so that the cAMP signaling is present in cell1), cell1 run ahead of cell2, and these cells shared the same circadian period (23.6 hr) due to the intercellular coupling. By contrast, under the condition that $v_\beta = 0$ (which corresponds to the deletion of cAMP signaling from cell1), these two cells began to fluctuate mutually in phase with an elongated circadian period (24.4 hr). These results indicate that the deletion of cAMP signal at dawn leads to the loss of phase-leading cell and elongates the period of coupled oscillators, a situation similar to what was observed for *Rgs16*$^{-/-}$ mice.

In conclusion, our mathematical simulations support the notion that the functional changes in a small subset of neurons can affect the whole SCN property. This is consistent with a general concept made for coupled oscillators, which presumes a critical effect of local change on global property[63-67]. It is however, obvious that our model is not comprehensive enough to faithfully recapitulate the whole SCN function. In our model, we hypothesized the following two principles: (i) reciprocal coupling of the two oscillatory cells, and (ii) assignment of cAMP signaling at dawn to one of the two cells. The former is a condition widely used for the simulation of SCN intercellular network[7,53], and the latter reflects the heterogeneity of cells in regard to the cAMP-dependent expression of *cFos* at dawn under constant darkness (Fig. 4)[40,41] . These two conditions may be too simple to express the complexity of the whole SCN network. For instance, alternative cAMP pathways incapable of elevating *cFos* expression could also play a role in SCN physiology. The mode of cell-cell coupling used is also hypothetical. It is theoretically possible that without mutual coupling, the phases of dorsomedial cells could be located earlier than those of ventrolateral cells if they are independently entrained to a common 'reference' pacemaker neuron in the SCN, a hypothesis that needs to be experimentally verified[68]. It is also important to note that our model does not account for the light entrainment pathway to the circadian clock, focusing rather on the simulation of the autonomous generation of inter-cellular phase-relationship between the SCN neurons under constant dark conditions. It is therefore obvious that mathematical modeling of whole SCN function will necessitate further investigation of the intercellular network across the SCN.

Supplementary References

61 Doi, M. et al. Salt-sensitive hypertension in circadian clock–deficient *Cry*-null mice involves dysregulated adrenal Hsd3b6. Nature medicine 16, 67-74 (2010).

62 Mombaerts, P. et al. Visualizing an olfactory sensory map. Cell 87, 675-686 (1996).

63 Winfree, A. T. Biological rhythms and the behavior of populations of coupled

oscillators. Journal of theoretical biology 16, 15-42 (1967).

64 Pittendrigh, C. S. & Daan, S. A functional analysis of circadian pacemaker in nocturnal rodents. J Comp Physiol A 106, 291-331 (1976).

65 Gonze, D., Bernard, S., Waltermann, C., Kramer, A. & Herzel, H. Spontaneous synchronization of coupled circadian oscillators. Biophysical journal 89, 120-129 (2005).

66 Kuramoto, K. Chemical oscillations, waves and turbulence. (Springer, 1984).

67 Winfree, A. T. The Geometory of Biological Time. (Springer, 2000).

68 Webb, A. B., Angelo, N., Huettner, J. E. & Herzog, E. D. Intrinsic, nondeterministic circadian rhythm generation in identified mammalian neurons. Proceedings of the National Academy of Sciences of the United States of America 106, 16493-16498 (2009).